Quaternary Science Reviews 324 (2024) 108463

Contents lists available at ScienceDirect

Quaternary Science Reviews

journal homepage: www.elsevier.com/locate/quascirev

Growth of the sandy isthmus of tyre and ensuing relocation of its harbors

Gilles Brocard [a,b,*], Jean-Philippe Goiran [b], Arthur de Graauw [b], Stoil Chapkanski [b,d], Arnaud Dapoigny [c], Emmanuelle Régagnon [b], Xavier Husson [a,e], Aurélien Bolo [f], Kosmas Pavlopoulos [g], Eric Fouache [h], Ali Badawi [i], Jean-Baptiste Yon [a]

[a] HiSOMA, MOM, UMR 5189, CNRS, Université Lyon 2, France
[b] Archéorient, MOM, UMR 5133, CNRS, Université Lyon 2, France
[c] LSCE (Laboratoire des Sciences du Climat et de l'Environnement), UMR 8212, CEA-CNRS-UVSQ, Université Paris Saclay, Gif-sur-Yvette, France
[d] IDEES Laboratory, UMR 6266, CNRS, University of Rouen Normandy, Mont Saint-Aignan, France
[e] EVEHA Paris-Ivry, Ivry-sur-Seine, France
[f] INRAP Méditerranée, Nîmes, France
[g] Médiations, UMR 7264, Sorbonne Université Paris, France/Paris Sorbonne University Abu Dhabi, Geography and Planning Department, France
[h] Médiations, UMR 7264, Sorbonne Université Paris, France
[i] General Directorate of Antiquities, Sur/Tyre, Lebanon

ARTICLE INFO

Handling editor: A. Voelker

Keywords:
Tyre
Tombolo
Sandy isthmus
Egyptian harbor
Harbor relocation
Ancient port
Phoenicia

ABSTRACT

The renowned Phoenician city of Tyre was settled on a small coastal island from which it resisted invasions and sieges for centuries. In 332 BCE, the city was taken when Alexander-the-Great built a 750 m-long causeway to seize the island. The causeway interrupted longshore sediment transport, forcing sand to accumulate along the causeway, creating a isthmus that today still connects the island to the mainland. This isthmus is no less than 530 m wide and 13 m high. We studied the impact of isthmus growth on city development during Antiquity, by combining archeological data, core stratigraphy, and multibeam bathymetry to track the paleogeographic evolution of the land-facing coast of Tyre, from the Holocene marine transgression up to today. In Phoenician time (900-300 BCE), sea-level markers indicate that relative sea level lied more than 2.5 m below current sea level, defining a 1500 × 600 m rocky island, 450 m longer in the south than the modern rocky headland. Between the island and the mainland, diffracted/refracted waves built a submerged sand bank that rests on eroded transgressive lagoonal clays. Along the mainland-facing coast of Tyre Island, Phoenician walls were built on the emerged end of the sand bank. Middle infrared spectroscopy (MIRS) shows that the sand of the bank and its successor isthmus is made of carbonate clasts (90–100%). $^{36}Sr/^{37}Sr$ ratios further indicate that these are modern bioclastic sands. Coeval, heterogeneous clay-rich sediments were deposited between the rocky island, and the sand bank. We interpret these as harbor sediments, deposited behind buried and/or submerged Phoenician breakwaters. The sand bank inflated dramatically after the building of Alexander's causeway, rising 5 m during the Hellenistic and Roman periods. It rose another 4 m–8 m in successive stages during Byzantine and Medieval times, up to the 19th century. The rapid growth of the sandy isthmus after 332 BCE led to the demise and burial of the harbors that had been developed along the mainland-facing coast. The Phoenician southern harbor of Tyre appears to have been buried in Roman times during the repurposing of the SE corner of the island for monumental baths. We interpret this repurposing as a response to the growth of the sandy isthmus, and suggest that the northern Phoenician harbor was then relocated to its present position. Subsequent relative sea level rise led to the erosion of the landfill overlying the southern harbor, exposing the formerly buried port on the seafloor.

1. Introduction

The end of the Last Glaciation was accompanied by a rise in sea level from −125 m to within a few meters from the current sea level between 18 ka and 6.5 ka BP (Lambeck and Chappell, 2001). The slower rise in sea level that followed was propitious, during Antiquity, to the development of long-lived coastal cities and ports. Nonetheless, the stabilization of sea level also allowed the formation of highstand system tracts

* Corresponding author. HiSOMA, MOM, UMR 5189, CNRS, Université Lyon 2, France.
E-mail address: gilles.brocard@mom.fr (G. Brocard).

https://doi.org/10.1016/j.quascirev.2023.108463
Received 29 July 2023; Received in revised form 1 December 2023; Accepted 3 December 2023
Available online 14 December 2023

which development affected these coastal settlements. Ancient harbors generally remained in use for centuries, thus experiencing substantial coastline changes. Such changes often jeopardized the sustainability of ports that had initially been settled at the most favorable locations. Numerous ancient ports had to be abandoned in face of tectonic uplift or subsidence (Riddick et al., 2021; Stiros and Blackman, 2014), ground settling (Stanley et al., 2004), and, in most cases, under the pressure of shoreline progradation, fed either by direct ingress of fluvial sediments in estuaries and deltas (Müllenhoff, 2005; Salomon et al., 2012; Stock et al., 2013), or by accretion along the coast, down drift of river mouths (Giaime et al., 2018; Stefaniuk et al., 2005). Progradation-related abandonment was hastened onshore by the development of agriculture, and associated increase in soil erosion (Maselli and Trincardi, 2013). Offshore, sediment drift was affected by coastal development. Along the Levantine coast (Fig. 1), sand accreted updrift of the Roman port of Caeasarea Maritima, although it remains unclear whether accretion contributed to the decline of the harbor (Raban et al., 2009). More impactful was the erection of two causeways by Alexander-the-Great: the 1100 to 1,300 m-long Heptastadion of Alexandria, a causeway built to protect its harbor (de Graauw, 2000), at the cost of substantial siltation (Goiran et al., 2015), and the causeway of Tyre (Fig. 1), built to seize the city of Tyre, which stood on an island. The effects of that latter causeway on coastal dynamics have been investigated in earlier studies which all showed that an enormous amount of sand accumulated on the causeway (Carmona and Ruiz, 2004; Marriner et al., 2007; Nir, 1996). Here we investigated what were the effects of this accumulation on the harbors of Tyre, and how the Tyrians coped with it. To achieve this, we bring together new and preexisting geological data, and combine them with available archeological data.

Tyre was one the most prestigious Phoenician cities, and was a major sea power during Antiquity. Built on an island, the city remained impregnable until it was besieged by Alexander-the-Great in 332 BCE. The earliest buildings excavated on the island date back to the Early Bronze age (~2500 BCE), which is regarded as permanently settled since at least 1600-1200 BCE, during the Late Bronze Age (Aubet, 2020; Bikai, 1978). The city became a prominent Phoenician city-state between the 9th and 6th centuries BCE, settling prestigious colonies around the Mediterranean Sea, such as Carthage and Leptis Magna (Carayon, 2005). It went under Persian rule in 572 BCE, before being conquered by Alexander-the-Great in 332 BCE. Monumental archeological remains erected during the subsequent Hellenistic, Roman, Byzantine, and Medieval periods (Aubet et al., 2016; Charpentier and Duvette, 2010, 2014; Kahwagi-Janho, 2016) led to its inscription on its archeological remains on the UNESCO World's Heritage list in 1984.

Ancient writers (Arrian II, 24; Strabo XVI,2,23) report that the island-city possessed two harbors (Fig. 2). The northern harbor opened toward the Phoenician city of Sidon and has been therefore referred to as the Sidonian Harbor, more properly the Port of Astronoe (Aliquot, 2020). The southern harbor opened toward Egypt and was referred to as the Egyptian Harbor. The location of the two harbors has been the subject of speculations since the 17th Century (Carayon, 2005; Renan, 1864–1874). The submarine excavation of a large, 4-6th Century BCE breakwater north of the city (Castellvi et al., 2007; Noureddine and Mior, 2013), and the discovery of 250 BCE to 500 CE harbor sediments behind this breakwater (Marriner et al., 2006) demonstrated the existence of a northern harbor (Fig. 2) under the modern harbor of Tyre repeatedly, if not permanently, throughout Antiquity.

The location of the southern harbor is more elusive. Renan, 1864–1874 envisioned it as an extensive structure now located offshore, south of the former island. Subsequent diving surveys identified submerged manmade structures on the seafloor within 150 m of the former island (El-Amouri et al., 2005; Frost, 1971). Poidebard (1939) led a pioneering diving exploration of these structures. He interpreted them as former breakwaters that enclosed a harbor with two entrances. The geographic area enclosed within these structures is therefore frequently referred to as the "Southern Harbor". Therefore, for consistency and convenience, we hereafter refer to that same area as the Southern Harbor, regardless of its actual purpose. These breakwaters have also been viewed as seawalls protecting a polder-like area that hosted an urban district (El-Amouri et al., 2005; Frost, 1971; Renan, 1864–1874).

The development of Tyre was profoundly affected by the construction of a causeway by Alexander-the-Great in 332 BCE, built to seize the city. This reportedly 750 m-long[1] and 60 m-wide causeway was laid over a submarine shoal less than 5.4 m deep.[2] This shoal was interpreted as a sandbank, formed by the accretion of sand in the lee of the island, under the effects of the refraction and diffraction of waves around the island (Carmona and Ruiz, 2004; Marriner et al., 2008a; Nir, 1996). The causeway interrupted longshore sand transport, forcing sand to accumulate along the causeway, rapidly creating an emerged sandy isthmus (or tombolo), linking the island to the mainland (Marriner et al., 2008a; Nir, 1996).

This sandy isthmus rapidly inflated during the centuries following the construction of the causeway. Today, its width is 530 m at its narrowest (Fig. 2), and it rises 13 m above sea level (asl). It thus stands higher than both the former island of Tyre to the west (+12 m) and the coastal plain to the east (+5–6 m). By early Imperial Roman times, monumental buildings had been built over most of its surface. Their layout implies that the isthmus was by then nearly as wide as today. Therefore, the isthmus had completely reshaped the eastern coast of Tyre Island within 3–4 centuries after the construction of the causeway, spurring a radical transformation of the city.

The magnitude of these changes and their impact on the city have long been noticed (Carmona and Ruiz, 2004; Nir, 1996), although no clear description of these effects is available yet. Here we aim at better assessing this impact, by combining geological and archeological markers that help us understand the evolution of the isthmus and coeval urban development. We concentrated our study on the east coast of Tyre Island, which was the most strongly impacted by these changes. New radiocarbon dating, Mid-Infrared Spectroscopy, and strontium isotopy are used to understand the provenance of the sands that make up the isthmus, and to assess the pace of accumulation of the sand between the island and the mainland. New land surveys were conducted on former coring sites and on offshore structures. These topographic data, the coring data, and recently-acquired offshore bathymetric data were then combined to reconstruct the topographic evolution of the land-facing coast of Tyre, from the formation of the island following the Holocene marine transgression, up to its burial within the sands of the isthmus. With this synthetic data on coastal dynamics, we discuss the repurposing of manmade structures observed along the east coast of Tyre Island.

2. Methods

2.1. Sediment cores

We conducted radiocarbon dating, chemical analyses, and isotopic analyses on seven previously extracted sediment cores of peculiar interest for this study, as they track the former eastern coast of Tyre Island (Fig. 2, Tables S1–1). Among these, the three southernmost cores (TYR1-3) are located in the immediate vicinity of the archeological site of Tyre-City, an area that features Roman-Byzantine monumental baths (Charpentier and Duvette, 2014). Core TYR4 was extracted next the crusaders' cathedral. Two cores (TYR5-6) were collected farther north in a densely urbanized area. Core TYR7 was collected in the Hellenistic-Roman Northern Harbor (Marriner et al., 2005). Sediment extraction was halted upon reaching either bedrock in TYR1 (8 m), TYR3 (8 m), and TYR7 (7 m), or lagoonal clays (Marriner et al., 2007) in cores TYR2 (9 m), TYR4 (18 m), TYR5 (19 m), and TYR6 (18 m).

[1] Four stades: Diodorus Siculus, Hist, 17, 7; Quintus Curtius Rufus, Hist, 4, 2; However, 700 paces: Pliny, Natural History V, 17.

[2] "Three fathoms": Arrian, Anab, 2, 18.

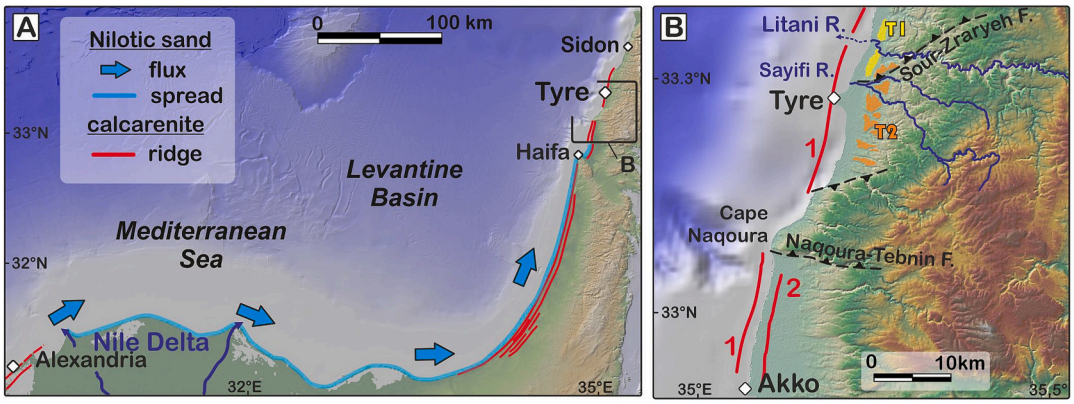

Fig. 1. Tyre and coastal sediment drift along the coast of the Eastern Mediterranean Basin. Topographic and bathymetric data: https://www.geomapapp.org. Panel A: map showing how longshore drift leads to the spreading of Nilotic sands along the Levantine coast, and the location of the main complexes of calcarenite ridges (Zviely et al., 2007). Red lines: onshore/partially emerged Pleistocene calcarenite ridges (Mauz et al., 2013; Stanley and Hamza, 1992; Tsoar, 2000). Panel B: Distribution of recent/active faults, calcarenite ridges and marine terraces T1 and T2 near Tyre (from Goiran et al. (2021), modified). Solid red lines 1 and 2: calcarenite ridges and their geomorphologic correlation astride Cape Naqoura.

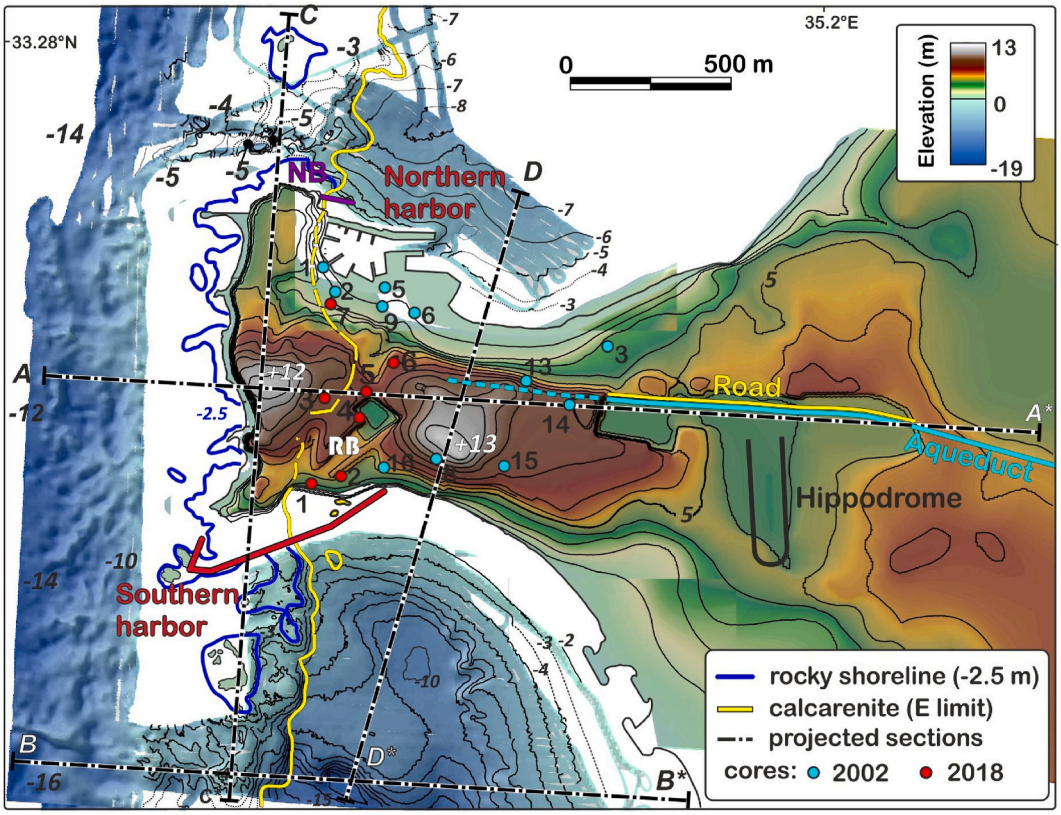

Fig. 2. Relief of the peninsula of Tyre and surrounding seafloor. NB: Northern Breakwater, RB: Monumental Roman Bath. Location of 2002 cores from Marriner et al. (2007). Onshore and offshore contour line spacing: 1 m. Projected sections A-A* and B-B* displayed on Fig. 7, sections C-C* and D-D* on Fig. 8.

2.2. Land surveying of the sandy isthmus

Land surveying was conducted in order to reassess the elevation of the coring sites with respect to sea level, and to precisely determine the depth of manmade structures that document relative sea level rise near the present-day shoreline (Goiran et al., 2021), These were measured relative to some of the buildings located onshore close to the shoreline (Charpentier and Duvette, 2014). The elevation of the coring sites was determined by DGPS and by total station leveling. The depth of the offshore markers was determined using a total station aiming at a partially submerged target (Suppl. Information S1).

2.3. Extraction of onshore and offshore topography

Onshore and offshore topographic and bathymetric data were combined in ArcGIS 10.8 to document the general morphology of the peninsula. The topography of its emerged part is provided by street-level elevation points recorded in the cadastral database of Tyre. Farther inland, within the coastal plain, elevation data come from pre-urbanization contour lines digitized on the 1967 edition of the Sour topographic quadrangle (scale 1:20,000, *Direction des Affaires Géographiques du Liban*). The contour lines were converted into elevation points with a 15 m-spacing along the lines. A nearest neighbor

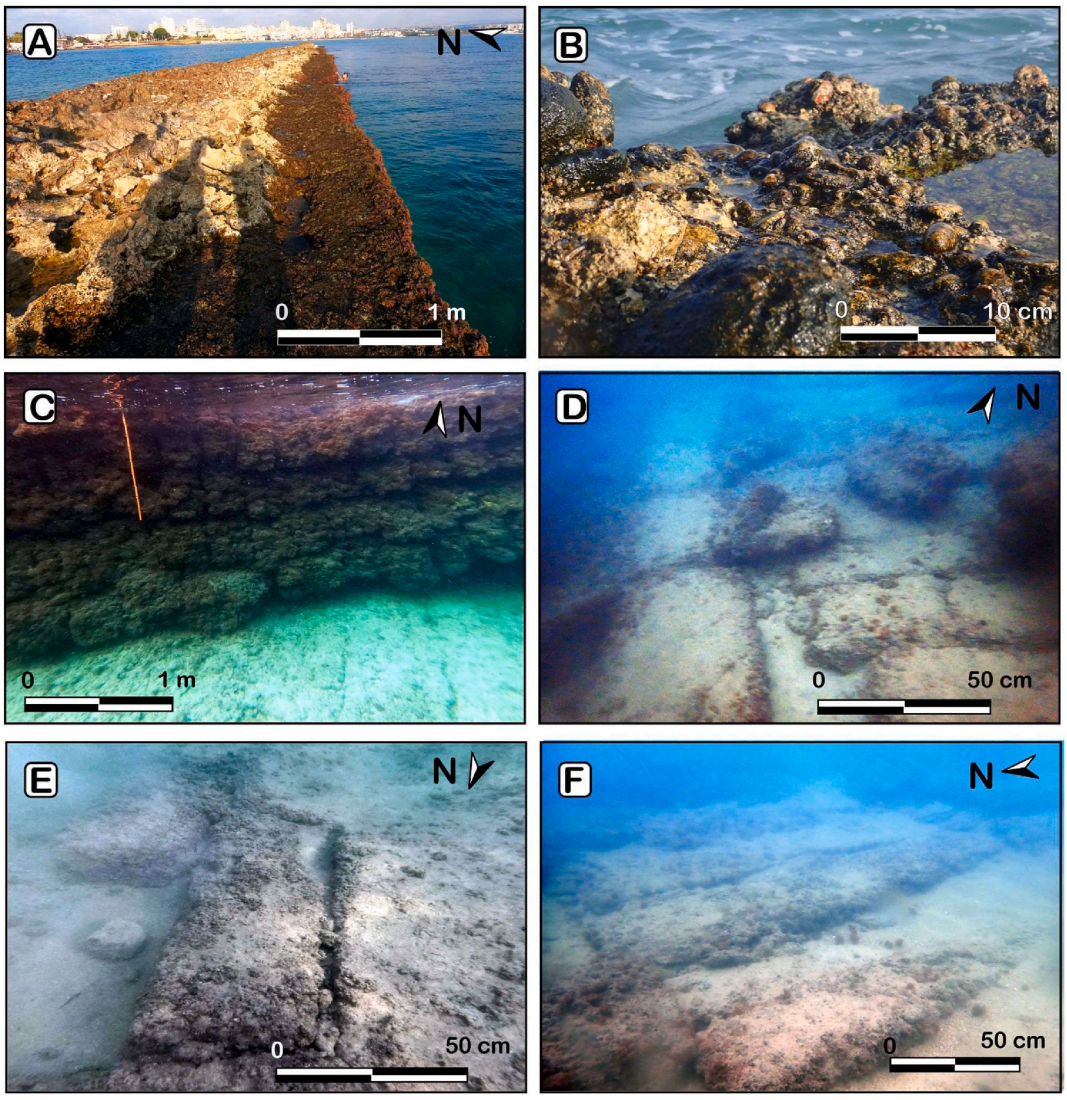

Fig. 3. Photographs of manmade markers of relative sea level located in the Southern Harbor (from Goiran et al. (2021), modified). A: Roman sea wall st1016 (El-Amouri et al., 2005), made of calcarenite headers, clad with concrete (Poidebard, 1939). B: detailed view of a seawall made of bulk concrete (*Opus Caementicium*). C: submerged calcarenite headers of seawall st1016, resting on the barren calcarenite basement. D: calcarenite headers and stretchers of the Quay of the Spring (Poidebard, 1939), st1027 (El-Amouri et al., 2005). E: flooded quarry floor (Q2) st1004 (El-Amouri et al., 2005). F: particularly long headers of the E-W breakwater (M) st1101 (Goiran et al., 2021). See Fig. 4 for locations. Credits: G. Brocard.

interpolation using all elevation points was then used to produce a 5 m-resolution DEM covering the entire peninsula at street level (Fig. 2). Topographic profiles (Fig. 2) were extracted from this surface, and core data were projected on these profiles to produce geological cross-sections of the isthmus. The surface was also used to calculate the volume of the sand stored in the isthmus (see section 2.4).

Offshore bathymetric combine a 0.25 m-resolution multibeam DEM (MarEA/EAMENA database, data GEOARCH-0000114) acquired by the General Directorate of Lebanon with support from the Honor Frost Foundation, to more extensive satellite imagery-derived bathymetric estimates (Westley, 2021).

2.4. *Theoretical sand fluxes, tombolo growth rate, and equilibrium size*

Growth-rate estimates of the sandy isthmus vary substantially (Marriner et al., 2008a; Nir, 1996). Here we conducted a new assessment based on an estimate of the annual influx of sand to the peninsula, and estimates of the volume of sand stored in the isthmus. The volume is based on the reconstruction of the morphology of the isthmus at three time steps: at the time of inception of sand accumulation, in 332 BCE, and today. The sand influx is assumed to be driven by longshore sediment transport (LST), which is the net annual sediment flux parallel to the mainland coast. The strength of this transport is a function of the angle between dominant wave crests and the coastline. Weather data and coastal dune morphologies at Tyre document a predominance of south-westerly over northwesterly winds, resulting in a net transportation of sand toward the north (Nir, 1996; Sanlaville, 1977). We calculated the LST transport capacity at Tyre using the CERC formula (US Army Corps of Engineers, C.E.R.C, 1984). It was applied to LST fluxes at Haifa (Zviely et al., 2007) with a correction for the decrease in wave incidence along the coastline from Haifa to Tyre (Supplementary Information S2).

The sandy isthmus rests on a substrate composed of transgressive lagoonal clays (Marriner et al., 2007) and of calcarenite at both ends. The total volume of sand in the isthmus is calculated as the difference in elevation between the modern surface of the isthmus (map S2.3) and the elevation of the underlying clays and calcarenite (map S2.1). The elevation/depth of the submarine shoal on which Alexander-the-Great's causeway was built is estimated from the location of the 300 BCE isochron within the sediment cores extracted along the peninsula (map

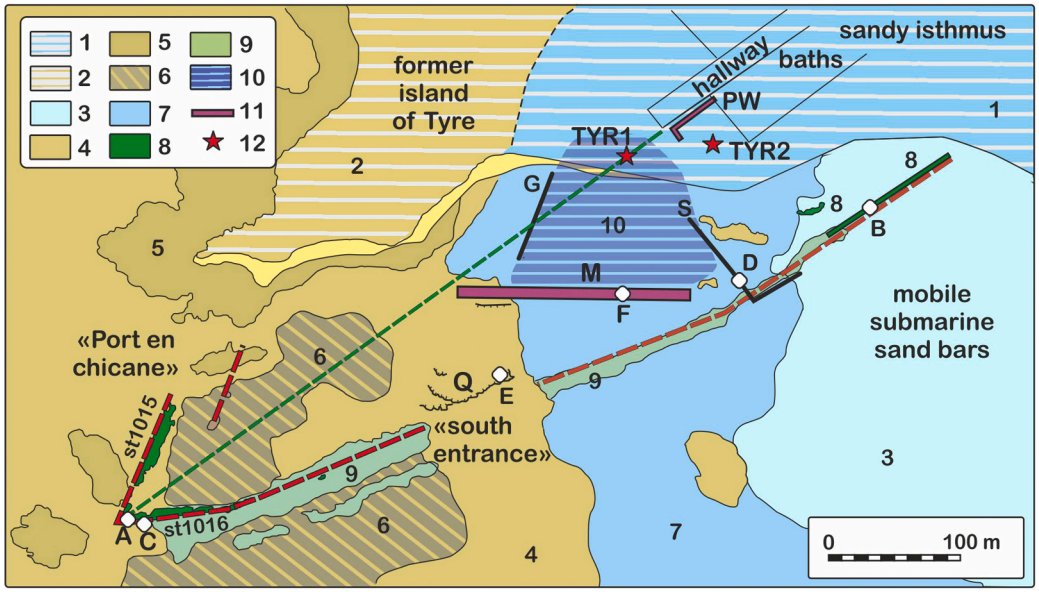

Fig. 4. Distribution of manmade structures, bedrock and sediments within the Southern Harbor. Red dashed line: Poidebard (1939)'s Southern Harbor enclosure. Green dashed line: axis of the monumental Roman baths. Formations: 1: emerged part of the sandy isthmus, 2: emerged land over calcarenite bedrock (wherever bedrock is above −2.5 m), 3: submarine part of the sandy isthmus, 4: submerged outcrops of calcarenite, 5: shore platform cut into calcarenite (mostly manmade), 6: natural block pavement over calcarenite, 7: natural block pavement over marine sediments, 8: roman concrete (*opus caementicium*), 9: rubble mound dyke, 10: proposed harbor basin, 11: Phoenician structure, 12: sediment cores. A to F: locations of photographs on Fig. 3. G: structure st1023 (El-Amouri et al., 2005), M: E-W Phoenician-like breakwater (Goiran et al., 2021), Q: quarries in calcarenite, S: Quay of the Spring (Poidebard, 1939), PW: Phoenician Wall (Charpentier and Duvette, 2014). From Goiran et al. (2021), modified.

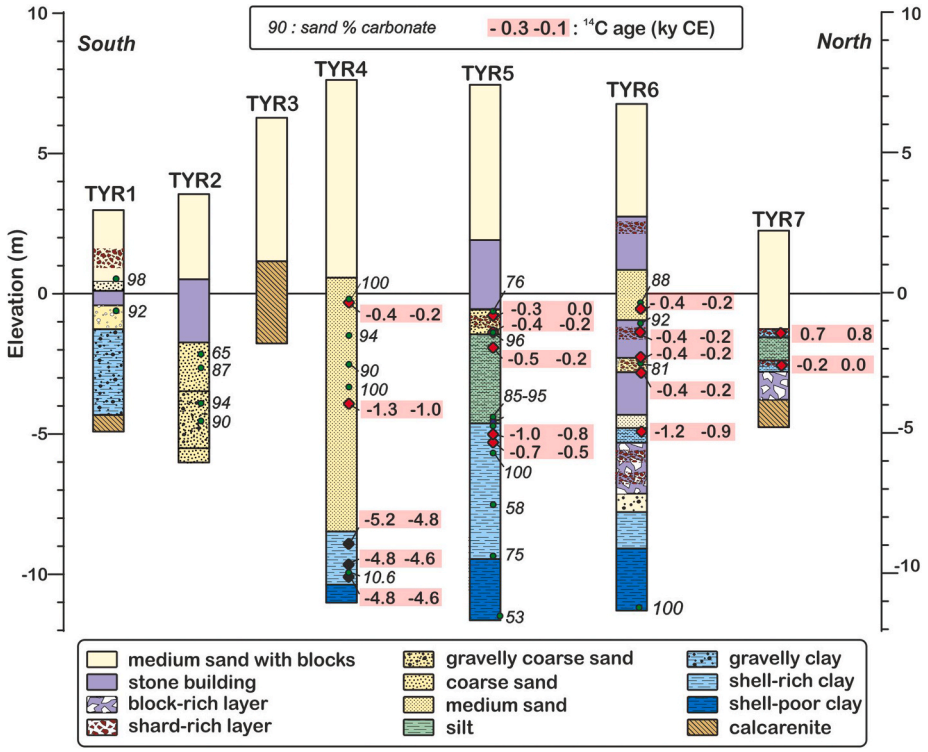

Fig. 5. Distribution of MIRS and ^{14}C samples along the stratigraphic logs of cores TYR1-7.

S2.2). We assumed that the submerged section of the sand bank has a length of 750 m, based on historical reports (see introduction). The difference in height between the 300 BCE reconstruction (map S2.2) and the modern topography (map S2.3) provides the volume of sand deposited since 300 BCE. This volume was divided by our LST estimate to calculate the time necessary for the isthmus to reach its present-day size.

2.5. Radiocarbon dating

Seventeen radiocarbon dates were obtained from cores TYR4-7 (Tables S3–1). Samples consist of terrestrial plant and animal remains

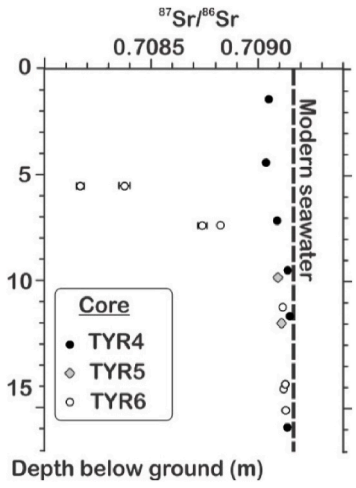

Fig. 6. Strontium isotopic ratios in carbonates sand, isthmus of Tyre. Dashed line: modern sea water ratio (Ohno and Hirata, 2007).

(charcoal, plants, bones, and seeds), with the exception of one marine gastropod. AMS target preparation was conducted at the Centre de Datation par le Radiocarbone of Lyon (Ar-Ar laboratory, University of Lyon 2, France). Isotopic ratios were measured on the ARTEMIS AMS facility, UMS 2572, at the LMC14 laboratory, Saclay, France. These ages and earlier published ages (Tables S3–2) were calibrated using the Oxcal online calibration software v 4.4 (https://c14.arch.ox.ac.uk/oxcal.html), using the calibration curve of Reimer et al. (2020) for terrestrial samples and the calibration curve of Heaton et al. (2020) for marine samples and no (unconstrained) local departure (ΔR = 0).

2.6. Sand composition by mid-infrared spectroscopy (MIRS)

Mid-infrared (MIR) light (4000-450 cm^{-1}) is particularly well adapted to the quantification of the concentration of carbonates (Henry et al., 2017; So et al., 2020), clays (Madejova and Komadel, 2001), quartz (Bertaux et al., 1998), a few other tectosilicates, and sulphates (Müller et al., 2014). Here we used mid-infrared absorbance spectroscopy (MIRS) to analyse the mineral composition of 24 sand and sandy clay samples collected in cores TYR1 (n = 2), TYR2 (n = 4), TYR4 (n = 5), TYR5 (n = 9), and TYR6 (n = 4). Their composition was measured using a FT-IR Frontier Spectrometer from 4000 to 450 cm^{-1}, in 2 cm^{-1} steps, at the analytical platform of Archéorient – UMR 5133 at Jalès, Ardèche, France (Suppl. Information S4).

The absorbance peaks of calcite (2,512 cm^{-1}), dolomite (2,525 cm^{-1}) and aragonite (2,501 cm^{-1}) where identified from the location of such peaks in a previously established pure mineral spectra database (Chapkanski et al., 2021). Spectra were pre-treated using the Kubelka-Munk function. The total amount of carbonates in the samples was obtained by combining the absorbance areas of the three aforementioned peaks, in the region between 2,542-2,493 cm^{-1}. The total absorbance intensity was then converted into weight concentrations using linear regressions established using pure mineral synthetic mixtures (Chapkanski et al., 2022).

2.7. Carbonate sand strontium isotopic composition

^{87}Sr (strontium) is produced by the disintegration of a parent ^{87}Rb (rubidium) isotope with a half-life of 48.8 Gy. The relative abundances of strontium isotopes evolve over geologic time by progressive addition of radiogenic ^{37}Sr. The $^{37}Sr/^{36}Sr$ of sea water has progressively increased since Jurassic times. The $^{87}Sr/^{86}Sr$ composition of marine

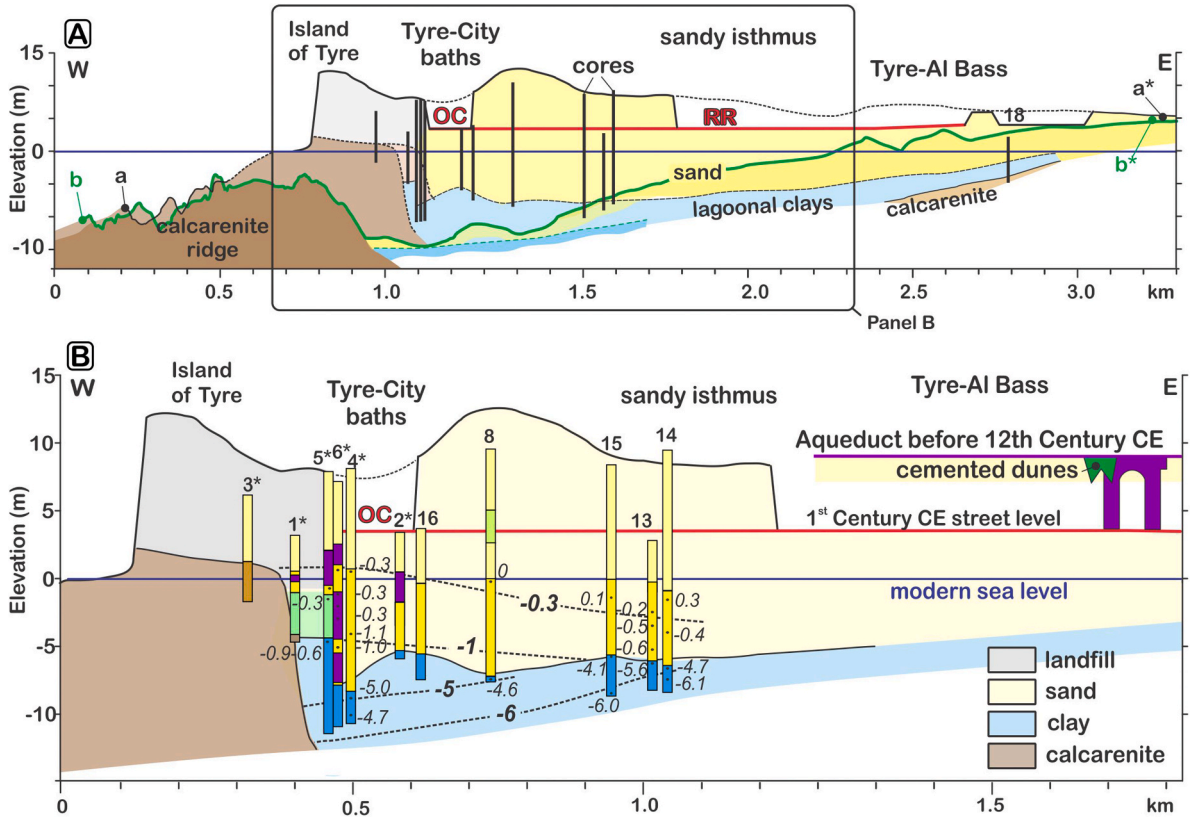

Fig. 7. E-W section through the peninsula. A: sketch geologic section along the peninsula (a-a*, black solid line, and dashed-line: pre-excavation topography), and along a parallel transect (b-b*) south of the peninsula (location on Fig. 2). B: geological section (from projected cores) at the junction between the tombolo and the east coast of Tyre. Core numbers without *: TI-XVI (Marriner et al., 2005, 2007, 2008b) and with *: TYR1 to 8. Numbers in italic: ^{14}C ages in ky CE. OC: octogonal church, RR: Roman road.

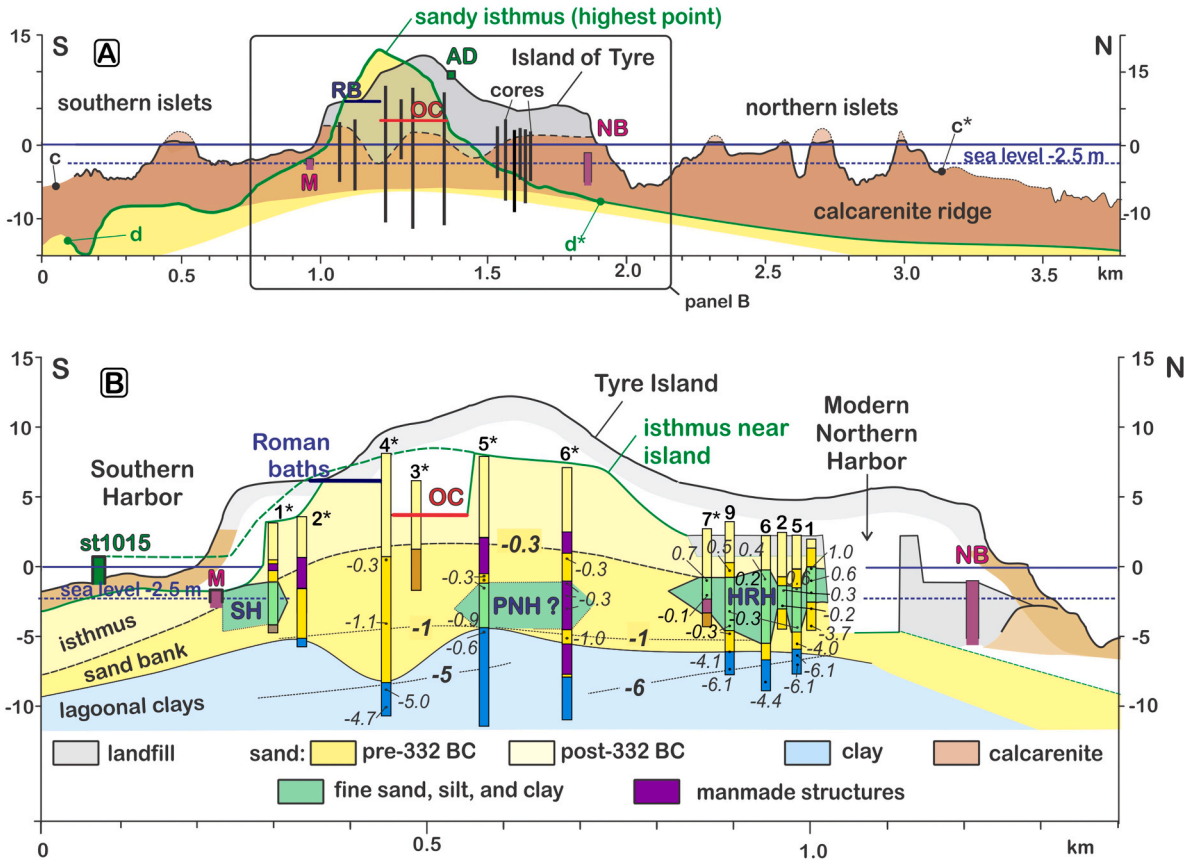

Fig. 8. N-S cross-section across the sandy isthmus and the island of Tyre. A: sketch geologic section across the island (c-c*, black solid line), and across the sandy isthmus (d-d*) (location on Fig. 2). B: geological cross-section (from cores projected on the section) along the east coast of the island of Tyre. Core numbers: TYRI to XVI (Marriner et al., 2005, 2007, 2008b) and (*): TYR1 to 8. Numbers in italic: ^{14}C ages in ky CE. AD: Aqueduct, OC: octogonal church, HRH: Hellenistic-Roman northern harbor, M: east-west breakwater (Fig. 4), NB: northern Phoenican breakwater, PNH: proto-northern harbor, SH: Southern Harbor, st1015: Roman-Byzantine structure of the southern harbor (Fig. 4).

carbonates reflects the composition of seawater at their time of crystallization. $^{87}Sr/^{86}Sr$ in carbonates has therefore been used to conduct stratigraphic correlations and marine carbonate dating (Elderfield, 1986). It has also been used as a tracer of rock source type/age (Bayon et al., 2021).

Here, we use this ratio to determine the provenance of the carbonate sands present in the isthmus of Tyre. The carbonates could come from nearby rivers that deliver sediment to the Lebanese coast. Source rocks in their catchments include Jurassic and Cretaceous limestones, Eocene marly chalks, and Miocene limestones. Another source is cemented Middle-Late Pleistocene (Dodonov et al., 2008; Mauz et al., 2013) calcarenite, variously referred to *ramleh* or *kurkar*, that blankets the coastline north and south of Tyre and the submerged ridge of Tyre (Badawi, 2016). A last source of carbonate is represented by bioclastic sands currently produced on the seafloor around Tyre (Castellvi et al., 2007).

Fourteen samples were selected from cores TYR4, 5, and 6 (Table S4-1). The sand fraction was extracted at the analytical platform of Archéorient – UMR 5133 at Jalès, Ardèche, France. Sample preparation was conducted at the Laboratoire des Sciences du Climat et de l'Environnement (LSCE) in Orsay, France. The isotopic composition was measured at the LSCE on a ThermoScientific ™ Neptune Plus™ Multi-Collector Inductively Coupled Plasma Mass Spectrometer (Supplementary Information S4).

3. Results

3.1. Ancient layout of tyre island and surrounding manmade structures

The land surveys (Tables S1–1) provided a better understanding of the relationships between geological and archeological elements. Offshore, they allow an assessment of the elevation of flooded structures relative to the structures unearthed onshore. The offshore leveling confirms earlier estimates of the depth of Phoenician quarry floors (Q1-Q3, st1002-1004-1005 (El-Amouri et al., 2005; Goiran et al., 2021)). These indicate that relative sea level has risen at least 2.5 m since the calcarenite was quarried there. We used the recently acquired multi-beam bathymetric data (MarEA/EAMENA database, data GEOARCH-0000114) to delineate the rocky coastline of Tyre Island when relative sea level was 2.5 m below modern sea level. The resulting island is 1,500 m long and 600 m wide (Fig. 2). Its perimeter of 4 km is consistent with its reported perimeter of 22 stadia.[3] The island does not extent much farther than today to the north, contrary to what was previously thought, based on conventional bathymetry (Marriner et al., 2007), but instead extends 400–600 m farther to the south. In the west, the shoreline of the island is highly festooned, exhibiting a series of headlands and reentrants. The reentrants are currently buried onshore under archeological levels. They might extent all the way across the island and divide it into a series of 2–3 separate islets, similar in size and shape to the islets found north and south of Tyre along the submarine

[3] Plinius,5,17.

ridge (Fig. 2). The bedrock of the former island does not appear to rise much above present-day sea level. It is found at +1 m in core TYR3. It crops out along the base of the sea cliff of the west coast below the archeological levels, rising irregularly from +1.0 m in the north, to +1.5 m in the center, to +2.5 m in the south. The calcarenitic bedrock was intersected below −2.5 m in all the cores located along the east coast, providing an easternmost boundary for the location of the rocky shoreline, when relative sea level lied below −2.5 m. The east coast then most likely lied in the continuation of the landward-facing flank of the submarine ridge of Tyre, as revealed by the multibeam bathymetry (Fig. 2). The width of the rocky island would have been 400–600 m.

Most of the manmade structures built around the rocky core of the island are currently buried under the peninsula. A few of them, however, crop out on the sea floor north, west, and south of the former island (El-Amouri et al., 2005; Goiran et al., 2021; Noureddine and Mior, 2013). In the Southern Harbor area (Fig. 4), the depth of shore-perpendicular structures increases with increasing distance to the coastline, from −1.1 to – 2.8 m along G (Fig. 4, st1023 in El-Amouri et al. (2005)), and from −1.4 to −2.2 m along S (Fig. 4, Quay of the Spring in Poidebard (1939), st1027 in El-Amouri et al. (2005)). At their offshore termination, these two structures connect to shore-parallel breakwater M (Fig. 4, st1101 in Goiran et al. (2021)) which lies at −1.9–2.0 m. The offshore increase in structure depth corresponds to an increase in the distance to the bedrock and therefore, likely, an increasing thickness of underlying Holocene marine sediments. This is also observed along the 40 m-long Northern Phoenician Breakwater (Castellvi et al., 2007), which surface lowers from −1.2 to −2.0 m offshore and away from the bedrock, according to the multibeam bathymetry (MarEA/EAMENA database, data GEOARCH-0000114). Later built structures (st 1015, st 1016, 8 on Fig. 4) of likely Roman-Byzantine age (Goiran et al., 2021), are still partially emerged.

3.2. Burial of the east coast of tyre

The new radiocarbon ages are used to better constrain the structure of the sandy isthmus close to the rocky island, expanding a dataset of radiocarbon ages more widely distributed over the isthmus (Marriner et al., 2007). In core TYR7, the basement is encountered at −3.5 m, in close proximity to the rocky shoreline, inland of the previously identified northern harbor of Tyre (Marriner et al., 2005). In all other cores the basement is located much deeper, beyond −10 m in most cores. In cores TYR4, 5, and 6, the Holocene sequence starts between −8 and −10 m with the deposition of transgressive lagoonal dark clays between Tyre Island and the mainland (Marriner et al., 2007). Marine sands overlay these clays. They accumulated all the way up to sea level in cores TYR2, 4, 5, and 6. They tend to be coarser in the south, where well-rounded gravel is interspersed (TYR1, 2). In the cores located the closest to the former shoreline (TYR1,7) however, silty-clayey sand laps onto the calcarenite ridge as far up as −1.5 m. Artefacts become abundant in these layers at −0.5 m in TYR1, -1 m in TYR5, and -6 m in TYR6. The artefacts consist of pottery shards and construction blocks, the latter being made of local limestone, among which calcarenite predominates. Above sea level, all TYR cores are composed of a mixture of sand and construction blocks.

The radiocarbon ages (Fig. 5, Table S3-1 and S3-2) document the development of lagoonal conditions behind the ridge of Tyre by 5.0–4.5 ky BCE (TYR4), during the marine transgression. Quiet, clayey sedimentation occurred landward of the initially extensively emerged ridge of Tyre (Marriner et al., 2007). Quiet sedimentation persisted until the Late Bronze Age (1.2–0.9 ky BCE) next to Tyre Island, allowing the deposition of these massive clays as far up as −3 to -4 m (TYR5, 6). It cannot be excluded that clays were also deposited at the same time farther from the island, but in this case they were eroded before sand deposition, because an age gap of several thousands of years is observed between clay deposition and sand deposition. Sand deposition starts at – 8 m in TYR4, reaching −3.5 m by 1.2–0.9 ky BCE (TYR4, 6). Sand deposition continues to within −1.5 m of modern sea level at 380-200 BCE in TYR4, 400-220 BCE in TYR5, and 370-270 BCE in TYR6, when numerous construction blocks appear within the sands. The main archeological strata are found between −2.5 m and +6 m. In TYR5 they initiate in early Hellenistic time (400-220 BCE) at −1 m and are likely of Roman age (marble blocks) by +1 m. In TYR6, they start a −3 m and remain early Hellenistic or Persian (450-310 BCE) up to + 1 m and are likely Roman above (basalt blocks). Recovery was poor farther up in all cores, throughout an anthropogenic diamicton of dry sands and rubble. In TYR7, the bedrock is overlain by silty-clayey sands reminiscent of the northern Hellenistic-Byzantine harbor (Marriner et al., 2005), likewise deposited between −2.5 and −1 m in Roman-Byzantine times (163 BCE to 776 CE).

3.3. Theoretical growth of the sandy isthmus

The net transportation of sand calculated here is consistent with earlier findings of northward-oriented longshore transport (Nir, 1996; Sanlaville, 1977). This net direction of transportation is confirmed by the opening of all ports towards the north along the Levantine coast. This direction is consistent with the direction of the vast anticlockwise drift gyre that conveys sands from Cyrenaica in Libya to the Nile delta in Egypt, and then northward along the Levantine coast (Fig. 1A). In this gyre, Nile-derived sediments are transported as far north as the Gulf of Haifa, 40 km south of Tyre, which acts as a terminal sink. At Haifa, longshore drift moves 50–80,000 m^3 of sediments northwards every year (Zviely et al., 2007). The decrease in wave incidence angle from Haifa to Tyre results in a LST transport capacity reduced to 30,000-50,000 m^3/y at Tyre. This estimate is regarded as an upper value, because the actual flux may be restricted by sand availability in the source area, theoretically located between Haifa and Tyre.

Today's sandy isthmus has an estimated volume of 40 Mm^3, half of which was deposited in transgressive sand dunes above sea level. The reconstructed sandbank of 330 BCE has an estimated volume of 10 Mm^3, such that post-causeway sand accretion consists of 10 Mm^3 of sand deposited in the sea, plus 20 Mm^3 of sand deposited above sea level. At the present-day rate of long-shore transport, the post-causeway volume would have accumulated within 6–10 centuries, such that the isthmus would have reached its present-day size between the 300 and 700 CE, that is, during the late Roman-Byzantine period. Since then on, LST and wind transport allow sand to bypass the peninsula of Tyre without hindrance, such that the topography of the isthmus remains in equilibrium. Hydrographic charts from 1861 and from 1999 CE by the British Hydrographic Office support this equilibrium state hypothesis, as they do not indicate any significant change in the coastline shape (i.e., within ± 10 m) or in the depth of the seafloor.

3.4. Sand carbonate content, and Sr isotopic composition

The isthmus of Tyre is formed of a clean sand which MIRS analysis shows to be composed of 89 ± 11 % carbonate on average, with values ranging from 65 to 100% (Tables S4–1, Fig. 5). It is distinctively richer in carbonates than the sandy fraction of the underlying lagoonal clays, deposited before the sand bank (10–50% carbonate).

Most samples from TYR4, 5 and 6 cores display isotopic signatures close to that of present-day seawater, with a mean value of 0.709114 ± 6.8 10^{-5} (Tables S4–2, Figs. 5 and 6). A few samples above sea level in core TYR6 display a less radiogenic signature (Fig. 6), with a minimum value of 0.708170 (15). According to the global marine isotopic curve (McArthur et al., 2020), this later signature corresponds to Oligocene marine sediments. It is therefore likely a mixture of Quaternary bioclastic sand mixed with some of the numerous Eocene chalk blocks interested by the cores, ground by the coring device during coring operations.

4. Discussion

Mineralogical and isotopic data are first used to discuss the provenance of the sand that forms the bulk of the isthmus, which accumulation led to the burial of the Phoenician harbors (section 4.1). We then show how similar sand accumulated during the last interglacial to form the rocky ridge of Tyre, which makes Tyre an unusually-young island. This helped forming a particularly deep natural harbor in the lee of the island during the millennia following the Holocene marine transgression (section 4.2). We then present elements in support for the existence of early harbor protections along the east coast of Tyre Island (section 4.3) that have been buried during the growth of the sandy isthmus (section 4.4). We propose that their burial led to the relocation of the northern harbor of Tyre away from the growing isthmus, whereas the southern harbor was repurposed (section 4.5). Finally, we discuss the age of a substantial amount of relative sea level rise (2.5 m), which modified the shape of the former island; coastal erosion then exhumed the buried southern harbor, while the northern harbor remained buried beneath the isthmus (section 4.6).

4.1. Sand provenance: bioclastic production

Our MIRS analysis shows that the sand of the isthmus is similar in composition to the sand found in beaches and dunes along the mainland, where carbonates make up on average 70%–80% (Carmona and Ruiz, 2004; Nir, 1996; Sanlaville, 1977) of the sand fraction. Their $^{86}/^{87}$Sr isotopic composition further indicates that these marine sands formed during Quaternary times. This precludes a significant contribution of coastal rivers to the formation of the tombolo, as advocated before (Marriner et al., 2007, 2008a). These sands are either produced directly by modern organisms offshore (Castellvi et al., 2007) or by erosion of biocalcarenite along the submarine ridge of Tyre or along the mainland coast (Nir, 1996). At sea the calcarenite is covered by modern bioherms and only shows very localized marks of recent erosion (such as plucked blocks and marine potholes). Besides, the calcarenite headers used in the Southern Harbor seawalls (Fig. 3A) also show little erosion despite their age. Living organisms are therefore the most likely source of the sand feeding the tombolo (green algae, bryozoans, corals, annelids, gastropods and bivalves (Castellvi et al., 2007)). It is likely that the bioclastic sands are produced within 40 km south of Tyre, north of the Gulf of Haifa, which is regarded as terminal sink of Nilotic sediment and brought to Tyre by a short littoral cell initiating on rocky headlands 10 km south of Tyre (Nir, 1996).

4.2. A new island for a new harbor

Previous interglacial marine highstands stood within a few meters from the current highstand (Antonioli et al., 2004; Benjamin et al., 2017). Therefore, at places that undergo moderate amounts of coastal progradation or retrogradation, highstand coastal islands reform at the same place from one interglacial to the next, until they become either permanently attached to the land, or eroded away. Holocene sandy isthmuses therefore grow over predecessor marine banks or isthmuses, formed by the same wave refraction processes during previous interglacials in the lee of these islands. Lengthwise (Fig. 7) and crosswise (Fig. 8) geological sections of the isthmus of Tyre show that no such predecessor sand bank or isthmus exists. The Pleistocene basement plunges steeply below −10 m within 100 m of the island along its eastern flank (Fig. 7A), as does the submarine ridge offshore (Fig. 7B). It allowed the formation of a remarkable natural harbor during the Holocene transgression, owing to the absence any obstructing remnants of former isthmuses.

Tyre is therefore a new island that did not exist during the last interglacial. The calcarenite ridge of Tyre, with its abundant cross-stratifications, is similar to many other calcarenite ridges (Fig. 1A) found along Levantine coast (Dodonov et al., 2008; Mart and Belknap, 1991; Mauz et al., 2013). They are composed of lithified aeolian sand dunes over foredune ridge plains (Mauz et al., 2013; Tsoar, 2000). The ridge of Tyre extends underwater at least 25 km to the north of Tyre, and 10 km to the south, where it is interrupted by rocky headlands (Fig. 1B). South of these headlands, a similar calcarenite ridge that bears some islets stands at a similar distance from the coast (1, Fig. 1B). It stretches over 20 km as far south as Acre (Akko). The ridge lies seaward of another calcarenite ridge (2, Fig. 1B), emplaced during marine isotopic stage (MIS) 5.5 (Sivan et al., 2016). Imbricate, 97 to 58 ka-old calcarenitic ridges seaward of the MIS 5.5 ridge (Mauz et al., 2013) were emplaced during the first interstadials (5.3 and 5.1) during the early stages of the last glaciation. The offshore ridge north of Akko, emplaced seaward of the MIS 5.5 ridge, was therefore likely emplaced during interstadial 5.3 and 5.1. The ridge of Tyre, which rises 30 m above the seafloor therefore most likely formed during such interstadials, when sea level stood 20–30 m bsl (Benjamin et al., 2017). It is also consistent with the age of the flooded 99 ka calcarenite ridge further north, which supports the island and Phoenician city of Arwad (Dodonov et al., 2008). The sandy isthmus of Tyre developed in the saddle between the new island of Tyre and earlier calcarenitic beach deposits at the coast.

4.3. The first manmade harbors

Transgressive clays were deposited in the saddle between the ridge of Tyre and the mainland at the beginning of the marine transgression, between ~6.0 and 4.0 ky BCE, when the ridge of Tyre was still extensively emerged, sheltering a vast natural lagoon (Marriner et al., 2007). Sand deposition initiated around 4 ka BCE, when the calcarenite ridge became more widely submerged (Marriner et al., 2008a). Next to the island however, clay deposition persisted until the end of the Bronze age at ~0.9 ky BCE (core TYR4), despite the coeval deposition of sand farther offshore. Undated clay in core TYR1 indicates that a protected environment was present as far up as 1 m bsl (Fig. 5) in the Southern Harbor area (see section 4.5 for details). The proximity of the areas of clay deposition to the areas of sand deposition implies that manmade structures are present between them at least since the Bronze Age. The northern breakwater was built in the 6th-4th Centuries BCE (Castellvi et al., 2007), providing an indicative minimum age for harbor structures.

When sea level lied 2.5 m below current sea level, the contours of the rocky island (Fig. 2) did not extend farther north, but instead extended at least 450 m farther to the south, offering much better sheltering than today to the Southern Harbor area. Tyre reportedly possessed two harbors, one opening to the north, and one opening to the south (Arrian 2, 18–20). These two harbors were most likely located in the lee side of the island, along its most sheltered stretch of coast. By then, the marine sand bank had reached a large size (Fig. 8B). It can be expected, therefore, that in Phoenician time, these two harbors lied on the northern and southern flanks of this marine sandbank, opening respectively toward the north and toward the south, away from the shallow sand bank crest (Fig. 9A).

The distribution of ^{14}C ages in the sand (Fig. 7B) and of archeological structures provides clues on the probable location of the sandbank, and therefore, on the location of the harbors. Phoenician walls and wells rest on sand between cores TYR1 and TYR2 (Fig. 4), at a place where the rocky basement lies below −5 m (Fig. 5). We interpret this sandy area as the emerging salient of the sandbank at its termination toward the island. The distribution of ^{14}C ages suggests a location of the sandbank crest at the latitude of these walls, ~200 m south of the Roman triumphal road (Fig. 2). Its location is compatible with the greater former extent of the "-2.5 m island" in the south, which tended to focus the convergence of refracted waves farther south than today, south of the Roman road. Owing to their close proximity to the sandbank, these early harbors were strongly affected by the following inflation of the sand bank.

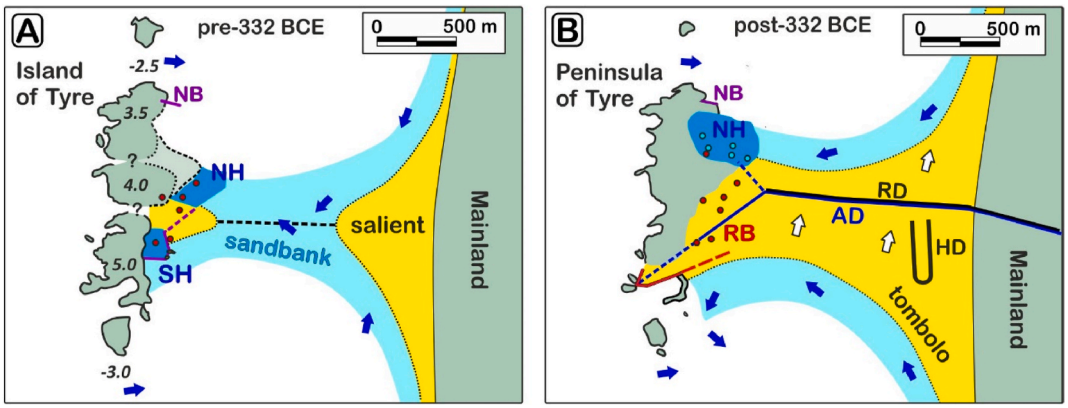

Fig. 9. Sketch maps showing the growth of the sandy isthmus of Tyre and its effects on harbors located along the east coast of Tyre. A: paleogeography before the building of the causeway; B: paleogeography by the 1st century CE. Arrows: net sand flux (blue: marine, white: terrestrial). AD: Aqueduct, HD: hippodrome, NB: northern breakwater, NH: northern harbor, RD; Roman triumphal road, SH: southern harbor, RB: Roman monumental baths. Numbers on panel A refer to the minimum, currently constrained elevation of the calcarenitic bedrock relative to sea level at −2.5 m. Red dots: cores TYR1-7. Blue dots: cores located in the Northern Harbor (Marriner et al., 2005).

4.4. Emergence and rise of the sandy isthmus

Radiocarbon dating documents an increase in the vertical growth rate of the submarine sand bank between the 8th or the 3rd centuries BCE and the 1st century BCE, during which its surface rose from −7.5 to −3.5 m (Marriner et al., 2007). This acceleration has been ascribed to sand accumulation along Nabucodonozor II's 6th century BCE causeway, followed by sand accumulation along Alexander-the-Great's causeway during the 4th century BCE (Marriner et al., 2007). The bank is believed to have been shallow enough to allow for the construction of these causeways (Marriner et al., 2007; Nir, 1996). The existence of Nabucodonozor's causeway, which is based on St Jerome's writings, is unsubstantiated (Renan, 1864–1874). Alexander's causeway is better documented. It was made of wood and stones taken from an urban area located on the mainland (Old Tyre). It was laid down on a bank which was, by then, no deeper than 5.4 m (Diodorus Siculus 17, 7). In the absence of ^{14}C dates in the sand overlying the causeway, the following growth of the bank can only be constrained using theoretical approaches. Nir (1996) calculated that sand influx to the bank was large enough for the isthmus to reach its current size by Roman time. Our own estimate of sand influx and of sand volume suggests that the isthmus reached its current size within 6–10 centuries of the construction of the causeway, that is, between 300 and 700 CE.

Archeological layers on the isthmus nonetheless provide a few additional milestones. The central hallway of the baths, which was built during early Roman Imperial time (1st Century CE) lies at + 6.0 m (Tables S1–1). Streets located nearby, around an octagonal church (5th Century), lie at +3.2–3.8 m (Tables S1–1). A 1 km-long triumphal Roman road straddles half the length of the isthmus (Fig. 2) at an elevation of +3.0–3.2 m (Kahwagi-Janho, 2016). A 450 m-long byzantine hippodrome lies at the same elevation, and so does the base of the piles of a 1st Century aqueduct (Kahwagi-Janho, 2016). This general accordance in elevation of Roman and Byzantine buildings indicates that the sandy isthmus had been levelled to +3–4 m by the 1st Century CE, indicating complete shoaling and rise to more than +3 m of the sand accumulation (Fig. 8B). The Roman aqueduct remained in use until the siege of 1,291 CE (Kahwagi-Janho, 2016). Large carbonate concretions developed below the aqueduct by leakage of calcium-rich waters (Fig. 8B), cementing dunes that abutted the aqueduct. The dunes had therefore reached the elevation of the aqueduct (≥+9 m) before the 12^{nd}/13th century. They still reached this elevation in the 1930s before the beginning of the archeological excavations (Poidebard, 1939). A last marker is provided by the ground floor of an Ottoman house at the highest point of the isthmus +13 m (Fig. 2), indicating that this elevation had been reached at the latest by the 19th Century CE. Maintaining harbors along the east coast of the island, in the face of this accumulation of sand, became likely excessively costly. The general leveling of the isthmus in Roman time, and the construction of numerous, extensive monumental buildings, as far as the ancient island, show that massive measures had been taken to redevelop the city according to this new layout. What coping strategy was then adopted to maintain maritime activities at Tyre?

4.5. Relocation and abandonment of the early harbors

Renan, 1864–1874 suspected that the ancient northern harbor of Tyre was located beneath the modern harbor, and that the southern harbor had silted up and fell in disuse. Coring confirmed the presence of a Hellenistic-Roman port basin beneath the modern harbor of Tyre (Marriner et al., 2005). The absence of Phoenician sediments in this basin was thought to result from their complete dredging during later times (Morhange et al., 2011). Cores TYR5-6, located farther south within the lee of the island, have intersected similar fine-grained sediments. Besides, TYR6 displays an outstanding alternation of blocks and silty clay starting 6 m below sea level. The age of these port-style layers is 1.1 ± 0.1 ka BCE at −3.5 m. They are overlain by sand layers of Hellenistic age between −1.5 and + 1 m. The cores therefore suggest that an earlier northern harbor existed before the Hellenistic harbor was used, at a naturally more sheltered location, also closer to the sandbank. Harbor sedimentation in the Hellenistic Harbor started at about the time when sedimentation stopped in the earlier harbor. Besides, it corresponds to the time when the sandy isthmus started to form. It seems therefore that it was decided to relocate the northern harbor farther away from the isthmus, in an area less affected by siltation.

The impact of the formation of the isthmus on the southern harbor is easier to observe in the Southern Harbor area, owing to the reduction in length of the island in the south, as a result of sea level rise. Such reduction resulted in a thinner accumulation of sand there, and even to some coastal erosion. Poidebard (1939) interpreted the conspicuous protective structures that enclose the Southern Harbour as breakwaters (Fig. 4) protecting a port that possessed two entrances, one in the south ("*Bab el Mina*"), and one in the west ("*Port en Chicane*"). Poidebard's Southern Harbor was later reinterpreted as an urban district protected by sea walls (El-Amouri et al., 2005; Frost, 1971). Within the harbour enclosure, a 130 m-long, 7-13 m-thick breakwater was later identified (Goiran et al., 2021). Its outer cladding of 1.5–2.0 m-long headers makes it resemble, in its layout and thickness, the 80 m-long, 12.7 m-thick northern Phoenician breakwater (6th-4th century BCE) and its 1.9

m–long headers (Castellvi et al., 2007). It is therefore interpreted as a breakwater that protected the Phoenician southern harbor of Tyre (de Graauw, 2022; Goiran et al., 2021). The extent of that harbor is constrained in the west by the calcarenite ridge of Tyre, and in the east by outcrops of calcarenitic sandstone (Fig. 4). To the north, it extends at least as far as core TYR1, in which clays are observed between −1.5 and −4 m (Fig. 5). To the NE, it does not extend as far as core TYR2, which only contains bioclastic sands of the sand bank. Phoenician walls, and the flooded "Quay of the Spring", located between these two cores, therefore appear to represent the eastern enclosure of the harbor.

The floor of the Roman baths stands 8 m higher than the top of the E-W breakwater (M, Fig. 7B). The close proximity of the bath to the southern harbor suggests that the Roman baths were developed partly on top of the port, and therefore represent a complete repurposing of the southern harbor of Tyre into a recreational area (Fig. 9). Two other traits of the Southern Harbor support this view.

First, the tops of the structures in the Southern Harbor that involve the use of *opus caementicium* (Fig. 3A and B) all stand 0.5 m above current sea level, whereas the tops of structures devoid of such concrete (Fig. 3D, F) typically lie at depths of 1.5–2.5 m. This difference in elevation suggests that the Roman seawalls/breakwaters are graded to a higher sea level than the other structures. No attempt was made to regrade the E-W Phoenician-style breakwater (M, Fig. 4) to Roman-time sea level, suggesting that the Phoenician harbor was in disuse by Roman time. Its abandonment, between Phoenician and Roman times, would have occurred while the sandy isthmus had started to form.

Second, concrete-clad structures st1015 and st1016, at the western termination of the Southern Harbor, form a triangle which bisector is aligned with the central axis of the monumental Roman Baths (Fig. 4), suggesting that the baths and these structures are parts of a common urban project. The two areas could have been connected across the Southern Harbor by a landfill, protected by the seawalls that enclose the "Southern Harbor" of Poidebard. It could have been laid during the general leveling of the isthmus in the 1st Century CE, using the sand reworked during the leveling.

4.6. Timing of sea level rise, and exhumation of the southern harbor

The ≥2.5 m rise in relative sea level documented in the Southern Harbor changed the size of the rocky island and of the sandy isthmus (Nir, 1996). The two early harbors were not equally affected, because the southern part of the island was more largely flooded than the northern part. Earlier studies suggest have most of the sea level rise occurred in Roman or Byzantine times (Marriner et al., 2005; Nir, 1996). Our observations concur with these earlier works.

In the Southern Harbor area, the elevation of the Roman walls relative to the Phoenician-like seawalls (~2.5 m higher on average) suggests that the rise in relative sea level occurred during the Hellenistic period. Along the west coast, fish tanks of tentative Roman-Byzantine age are flooded 40 cm above their functional level (Goiran et al., 2019), suggesting that the main phase of sea level rise was by then over. However, the functional level of the Roman seawalls that enclose the Southern Harbor area must be deeper, for these walls to efficiently protect any ground behind, suggesting that more substantial sea level rise occurred after their completion. The enclosure of the Southern Harbor was completed with more rudimentary rubble mound dykes (Fig. 4). These dykes abut on both sides the "Southern Entrance" of Poidebard's harbor, which is in fact a rocky shoal that rises to within 0.6 m of the sea surface. That the enclosure was not completed over the shoal suggests that the shoal was emerged, or shallow enough not to require protection when the rubble dykes were erected. These dykes contain Roman columns usually found in buildings erected in the 1st century CE, which indicates that they were built later, and that a substantial part, if not all, of the sea level rise has occurred as late as Byzantine time. Two additional lines of evidence support a late age of submersion. First, north of Tyre Island, an alignment of Roman columns 10–25 m south of the Phoenician Northern Breakwater (Noureddine and Mior, 2013) lies flush with the top of the breakwater, suggesting a flooding coeval to that of the southern harbor. Behind the breakwater, in the Hellenistic northern harbor, core TYR7 (Fig. 5) and earlier cores (Marriner et al., 2005) indicate that low-energy sedimentation ceased in 580–810 CE, after which coarser marine sands were deposited, starting at a depth of −1 to −2 m. This is consistent with the depth of submersion of the northern breakwater, and with a return of open sea sedimentation by flooding of the northern harbor in Late Byzantine time.

Relative sea level rise reduced the length of Tyre Island in the south, allowing for the sea to overflow the Southern Harbor enclosure, remove its landfill, and expose the underlying structures. The sandy isthmus being a dynamic feature, it was able to adjust its size and shape in response to sea level rise. Nir (1996) posited that sea level rose during Roman times, a time by which he considers that the isthmus had already reached maturity. In response to submergence, and to retrieve its equilibrium size, the isthmus would have resumed growing (Nir, 1996). We note, however, that the shrinking of the former rocky island of Tyre, and the general deepening of marine channels all over the ridge of Tyre should rather promote further contraction of the sandy isthmus. That contraction would have accompanied the unearthing of the southern harbor of Tyre, and the destruction of the northern Hellenistic harbor, whereas the earlier northern harbor remained buried beneath the sands of the isthmus.

5. Conclusions

New ^{14}C ages and geochemical data were combined with recently acquired stratigraphic, topographic, and bathymetric data to track the evolution of the east coast of Tyre Island, from its initial formation, at the end of the last glaciation, up to today. The east coast offered natural protection from waves and was the most suitable site for the settlement of the historical northern (Sidonian) and southern (Egyptian) harbors or Tyre.

The submarine ridge which emerges at Tyre is made of lithified sand dunes and beach deposits most likely formed during MIS 5.3 or 5.1 (100-75 ky BP), that is, during the early stages of the last glaciation, when sea level stood 20–30 m below its current level. The valley located between the ridge of Tyre and the mainland was filled by lagoonal clays during the early stages of the last marine transgression (6-4 ky BCE), forming a through-going natural harbor, unobstructed by earlier transgressive or regressive tracts of marine sediments.

As relative sea level rose, the ridge was submerged and the island shrunk in size. Stone quarry floors at 2.5 m below present sea level indicate that the island was occupied when the island was still 1,500 × 600 m large, and possibly no more than 4.5 m high. It extended mostly farther south than today, better protecting the area of the Southern Harbor.

The island provided a deep, protected shelter along its east coast. Sand deposition in that shelter, on a sand bank formed by refraction/diffraction of waves behind the island, became larger during the Late Bronze age, during the 2nd millennium BCE. We propose that the two harbors of Tyre were positioned facing away from the crest of this sandbank, which axis was located south of the Roman triumphal road, rather than below that road.

Mineralogical and isotopic analyses show that the sands of the isthmus are composed of modern marine carbonate bioclasts, originating from an area of production located within 40 km south of Tyre.

The data confirm the earlier finding that the sand bank became shallow enough for Alexander the Great to build his causeway on it. We find that the bank had already emerged at its termination on the island side.

The tombolo grew rapidly by marine sand accretion, and wind transport after the construction of the causeway. By Roman time, the tombolo was leveled at + 3–4 m over most of its length. The progressive abandonment of the isthmus allowed sand dunes to rise higher,

overtopping the Roman aqueduct at +9 m before it went into disrepair in the 13th century CE (Kahwagi-Janho, 2016).

The area of Poidebard (1939)'s Southern Harbor display an assembly of successive structures, which nature and arrangement over time indicates the reconversion of a Phoenician port into a Roman recreational district (monumental baths). The southern harbor basin is proposed to be north of newly identified Phoenician-like breakwater (M in Fig. 4). The timing of this repurposing coincides with the main phase of growth of the isthmus. It is concluded that repurposing was motivated by the obstruction of the southern harbor by the growing sandy isthmus.

Further north, the age of the sediments deposited in sheltered conditions of Phoenician age to the NE, and of Hellenistic-Roman age to the north under the modern harbor suggests that, likewise, an early northern harbor, located to the NE, was obstructed by the growing isthmus and relocated farther west, away from the isthmus, in Hellenistic times.

A 2.5 m + rise in relative sea level affected Tyre during Antiquity. A substantial part of this rise occurred in Hellenistic time, or/and Byzantine time, affecting both the isthmus and the repurposed parts of Tyre. It led to the erosion of the repurposed district of southern Tyre, while possibly also causing a decline of its northern harbor.

Contributions

Gilles Brocard (geologist): research design, data collection (land surveys), data synthesis, data interpretation, paleogeographic reconstructions, paper writing; Jean-Philippe Goiran (geoarcheologist): research design, grant collection, data collection (coring of cores TYR and T, core sampling), data interpretation; Arthur de Graauw (port engineer): data interpretation, sand flux modeling, paper writing; Stoil Chapkanski (engineer): analysis of sand mineralogy, paper writing; Arnaud Dapoigny (engineer): analysis of strontium isotopes; Emmanuelle Régagnon (topographer): DGPS land survey of cores TYR; Xavier Husson (topographer): DGPS land surveys of cores T; Aurélien Bolo (topographer): total station land survey of cores TYR and submerged structures; Kosmas Pavlopoulos (geographer-geomorphologist): research design, coring of cores TYR; Eric Fouache (geographier-geomorphologist): research design, coring of cores TYR and funding; Ali Badawi (director of archological site): research of historical data, administrative and logistical support; Jean-Baptiste Yon (historian, archeologist): research of historical data, paper writing, administrative and logistical support

All authors have read and approved the manuscript.

Funding

field surveys were supported by the INSH-Institut National des Sciences Humaines et Sociales [International mobility grant SMI, 2019], and by the Honor Frost Foundation -HFF [grant 2019]. Coring was supported by the Geoarchaeologia society (Net1901.org) [2018]. Sediment analyses were supported by the Agence Nationale pour la Recherche ANR [AquaTyr, 2022]. Dating was supported by the Archéorient Laboratory and the Mission Française Archéologique de Tyr [ARTEMIS, CNRS-SHS annual calls 2019, 2020].

Declaration of competing interest

The authors declare that they have no known competing financial interests or personal relationships that could have appeared to influence the work reported in this paper. Gilles Brocard reports financial support provided by French National Research Agency (grant ANR AquaTyr). Jean-Baptiste Yon reports finacial support provided by French National Research Agency (grant ANR AquaTyr). Jean-Philippe Goiran reports financial support for travel provided by the Honor Frost Foundation (grant 2019). and by the French Institute for Humanities and Social Sciences (CNRS-INSHS International mobility grant SMI, 2019). Jean-Philippe Goiran reports financial support for dating and sedimentary analyses provided by the Archéorient Laboratory, Maison de l'Orient et de la Méditerranée, University of Lyon 2, France (ARTEMIS, CNRS-SHS annual funding scheme 2019, 2020). Eric Fouache reports financial support for coring provided by the Geoarchaeologia society (Net1901.org, grant 2018). Jean-Philippe Goiran reports administrative support provided by the General Directorate of Antiquities and Cultural Heritage of Lebanon.

Data availability

Data are provided in the Supplementary Data File.

Acknowledgements

We thank the Directorate General of Antiquities (DGA) of Lebanon for its support. Field campaigns were validated by the DGA and conducted under the supervision of the Mission Française Archéologique de Tyr supported by the French Ministry of European and Foreign Affairs (MEAE) and the IFPO (Institut Français du Proche Orient).

Appendix A. Supplementary data

Supplementary data to this article can be found online at https://doi.org/10.1016/j.quascirev.2023.108463.

References

Aliquot, J., 2020. The port of Astronoe in Tyre. BAAL 18, 61–70.
Antonioli, F., Bard, E., Potter, E.-K., Silenzi, S., Improta, S., 2004. 215-ka History of sea-level oscillations from marine and continental layers in Argentarola Cave speleothems (Italy). Global Planet. Change 43, 57–78.
Aubet, M.E., 2020. Tyre before Tyre: the Early Bronze Age Foundation, Nomads of the Mediterranean: Trade and Contact in the Bronze and Iron Ages. Brill, pp. 14–30.
Aubet, M.E., Nuñez, F.J., Trellisó, L., 2016. Excavations in Tyre 1997–2015: results and perspectives. Berytus 56, 3–14.
Badawi, A.K., 2016. The ancient sources of building stones for the city of Tyre/Sur (Lebanon). Marmora 12, 141–158.
Bayon, G., Freslon, N., Germain, Y., Bindeman, I.N., Trinquier, A., Barrat, J.-A., 2021. A global survey of radiogenic strontium isotopes in river sediments. Chem. Geol. 559, 119958.
Benjamin, J., Rovere, A., Fontana, A., Furlani, S., Vacchi, M., Inglis, R.H., Galili, E., Antonioli, F., Sivan, D., Miko, S., 2017. Late Quaternary sea-level changes and early human societies in the central and eastern Mediterranean Basin: an interdisciplinary review. Quat. Int. 449, 29–57.
Bertaux, J., Froehlich, F., Ildefonse, P., 1998. Multicomponent analysis of FTIR spectra; quantification of amorphous and crystallized mineral phases in synthetic and natural sediments. J. Sediment. Res. 68, 440–447.
Bikai, P.M., 1978. The Pottery of Tyre. Aris Phillips.
Carayon, N., 2005. Contribution historique, archéologique et géomorphologique à l'étude des ports antiques de Tyr. BAAL-Bulletin d'Archéologie et d'Architecture Libanaises 53–60.
Carmona, P., Ruiz, J., 2004. Geomorphological and geoarchaeological evolution of the coastline of the Tyre tombolo: preliminary results. Bulletin d'Archéologie et d'Architecture Libanaises Hors-Série 1, 207–219.
Castellvi, G., Descamps, C., Kuteni, V.P., 2007. Recherches archéologiques sous-marines à Tyr.
Chapkanski, S., Brocard, G., Lavigne, F., Meilianda, E., Ismail, N., Darusman, D., Goiran, J.-P., 2022. Fingerprinting sources of beach sands by grain-size, using mid-infrared spectroscopy (MIRS) and portable XRF. Implications for coastal recovery along a tsunami-struck delta coastline. Catena 219, 106639.
Chapkanski, S., Goiran, J.-P., Rosa, C., Kay, S., de Graauw, A., Gallet, X., d'Ottavio, D., Keay, S., 2021. Infrared spectroscopic investigations of the Northern Mole of Portus, the Ancient harbour of Rome. Insights for stratigraphy and provenance of raw materials for construction. Mediterranean archaeology and archaeometry journal.
Charpentier, G., Duvette, C., 2010. Tyr: le complexe des bains et ses environs. BAAL-Bulletin d'Archéologie et d'Architecture Libanaises 146–159.
Charpentier, G., Duvette, C., 2014. Le complexe monumental de Tyr et les grands thermes de la fin du IVe s. In: Boussac, M.-F., Denoix, S., Fournet, T., Redon, B. (Eds.), 25 siècles de bain collectif en Orient. Proche-Orient, Égypte et péninsule Arabique. Βαλανεῖα, thermae, حمامات, Études urbaines. Institut Français de Damas, pp. 385–397.
de Graauw, A., 2000. Port engineering aspects of the magnus portus in Alexandria. Bull. - Int. Navig. Assoc. 31–42.
de Graauw, A., 2022. Ancient Port Structures, Parallels between the Ancient and the Modern. Méditerranée.
Dodonov, A., Trifonov, V., Ivanova, T., Kuznetsov, V.Y., Maksimov, F., Bachmanov, D., Sadchikova, T., Simakova, A., Minini, H., Al-Kafri, A.-M., 2008. Late Quaternary

marine terraces in the Mediterranean coastal area of Syria: geochronology and neotectonics. Quat. Int. 190, 158–170.
El-Amouri, M., El-Hélou, M., Marquet, M., Noureddine, I., Seco Alvarez, M., 2005. Mission d'expertise archéologique du port sud de Tyr, résultats préliminaires. Baal Hors Série II 91–110.
Elderfield, H., 1986. Strontium isotope stratigraphy. Palaeogeogr. Palaeoclimatol. Palaeoecol. 57, 71–90.
Frost, H., 1971. Recent observations on the submerged harbourworks at Tyre. Bulletin du Musée de Beyrouth 24, 103–111.
Giaime, M., Morhange, C., Marriner, N., López-Cadavid, G.I., Artzy, M., 2018. Geoarchaeological investigations at Akko, Israel: new insights into landscape changes and related anchorage locations since the Bronze Age. Geoarchaeology 33, 641–660.
Goiran, J.-P., Brocard, G., de Graauw, A., Kahwagi-Janho, H., Chapkanski, S., 2021. Evolution of sea level at Tyre during antiquity. BAAL 21, 305–316.
Goiran, J.-P., Chapanski, S., Régagnon, E., Pavlopoulos, K., Fouache, E., 2019. Preliminary results of rock-cut fish tanks evidence along the Tyre coast of Lebanon. Implication for ancient sea-level reconstruction. Baal 19, 259–265.
Goiran, J.-P., Tronchère, H., Salomon, F., Prieur, A., Djerbi, H., 2015. The geoarchaeology of ancient Mediterranean harbours in deltaic context. In: Carcaud, N., Arnaud-Fassetta, G. (Eds.), French Geoarchaeology in the 21st Century. CNRS Alpha, pp. 291–300.
Heaton, T.J., Köhler, P., Butzin, M., Bard, E., Reimer, R.W., Austin, W.E., Ramsey, C.B., Grootes, P.M., Hughen, K.A., Kromer, B., 2020. Marine20—the marine radiocarbon age calibration curve (0–55,000 cal BP). Radiocarbon 62, 779–820.
Henry, D.G., Watson, J.S., John, C.M., 2017. Assessing and calibrating the ATR-FTIR approach as a carbonate rock characterization tool. Sediment. Geol. 347, 36–52.
Kahwagi-Janho, H., 2016. Les monuments romains de Tyr extra muros: étude architecturale de la route antique, de l'arc monumental et de l'aqueduc. Ausonius éditions.
Lambeck, K., Chappell, J., 2001. Sea level change through the last glacial cycle. Science 292, 679–686.
Madejova, J., Komadel, P., 2001. Baseline studies of the clay minerals society source clays: infrared methods. Clay Clay Miner. 49, 410–432.
Marriner, N., Goiran, J., Morhange, C., 2008a. Alexander the great's tombolos at Tyre and Alexandria, eastern mediterranean. Geomorphology 100, 377–400.
Marriner, N., Morhange, C., Boudagher-Fadel, M., Bourcier, M., Carbonel, P., 2005. Geoarchaeology of Tyre's ancient northern harbour, Phoenicia. J. Archaeol. Sci. 32, 1302–1327.
Marriner, N., Morhange, C., Carayon, N., 2008b. Ancient Tyre and its harbours: 5000 years of human-environment interactions. J. Archaeol. Sci. 35, 1281–1310.
Marriner, N., Morhange, C., Doumet-Serhal, C., Carbonel, P., 2006. Geoscience rediscovers Phoenicia's buried harbors. Geology 34, 1–4.
Marriner, N., Morhange, C., Meulé, S., 2007. Holocene morphogenesis of alexander the great's isthmus at Tyre in Lebanon. Proc. Natl. Acad. Sci. USA 104, 9218–9223.
Mart, Y., Belknap, D.F., 1991. Origin of late Pleistocene submerged marine terraces on the outer continental shelf, northern Israel. Geo Mar. Lett. 11, 66–70.
Maselli, V., Trincardi, F., 2013. Man made deltas. Sci. Rep. 3, 1926.
Mauz, B., Hijma, M., Amorosi, A., Porat, N., Galili, E., Bloemendal, J., 2013. Aeolian beach ridges and their significance for climate and sea level: concept and insight from the Levant coast (East Mediterranean). Earth Sci. Rev. 121, 31–54.
McArthur, J., Howarth, R., Shields, G., Zhou, Y., 2020. Strontium isotope stratigraphy. Geologic Time Scale, pp. 211–238 (Chapter 7).
Morhange, C., Carayon, N., Marriner, N., 2011. Geoarchaeology of Byblos, Tyre, Sidon and Beirut. Geoarchaeology of Byblos, Tyre, Sidon and Beirut, pp. 55–66.
Müllenhoff, M., 2005. Geoarchäologische, sedimentologische und morphodynamische Untersuchungen im Mündungsgebiet des Büyük Menderes (Mäander), Westtürkei. (No Title).
Müller, C.M., Pejcic, B., Esteban, L., Piane, C.D., Raven, M., Mizaikoff, B., 2014. Infrared attenuated total reflectance spectroscopy: an innovative strategy for analyzing mineral components in energy relevant systems. Sci. Rep. 4, 1–11.
Nir, Y., 1996. The city of Tyre, Lebanon and its semi-artificial tombolo. Geoarchaeology 11, 235–250.
Noureddine, I., Mior, A., 2013. Archaeological Survey of the Phoenician Harbour at Tyre (Lebanon).
Ohno, T., Hirata, T., 2007. Simultaneous determination of mass-dependent isotopic fractionation and radiogenic isotope variation of strontium in geochemical samples by multiple collector-ICP-mass spectrometry. Anal. Sci. 23, 1275–1280.
Poidebard, A., 1939. Un grand port disparu: Tyr: recherches aériennes et sous-marines: 1934-1936. Geuthner.
Raban, A., Artzy, M., Goodman, B., Gal, Z., 2009. The Harbour of Sebastos (Caesarea Maritima) in its Roman Mediterranean Context. Archaeopress, Oxford.
Reimer, P.J., Austin, W.E., Bard, E., Bayliss, A., Blackwell, P.G., Ramsey, C.B., Butzin, M., Cheng, H., Edwards, R.L., Friedrich, M., 2020. The IntCal20 Northern Hemisphere radiocarbon age calibration curve (0–55 cal kBP). Radiocarbon 62, 725–757.
Renan, E., 1864-1874. Mission de Phénicie dirigée par Ernest Renan: Texte. Impr. impériale.
Riddick, N.L., Boyce, J.I., Reinhardt, E.G., Rothaus, R.M., Chomicki, K.M., McCarthy, F. M., 2021. Multi-proxy palaeoenvironmental record of coastal tectonic uplift and abandonment (ca. 6th c. CE) of Lechaion's inner harbour, ancient Corinth, Greece. Quat. Sci. Rev. 267, 107080.
Salomon, F., Delile, H., Goiran, J.-P., Bravard, J.-P., Keay, S., 2012. The Canale di Comunicazione Traverso in Portus: the Roman sea harbour under river influence (Tiber delta, Italy). Géomorphol. Relief, Process. Environ. 18, 75–90.
Sanlaville, P., 1977. ETUDE GEOMORPHOLOGIQUE DE LA REGION LITTORALE DU LIBAN. II.
Sivan, D., Sisma-Ventura, G., Greenbaum, N., Bialik, O., Williams, F., Tamisiea, M., Rohling, E., Frumkin, A., Avnaim-Katav, S., Shtienberg, G., 2016. Eastern Mediterranean sea levels through the last interglacial from a coastal-marine sequence in northern Israel. Quat. Sci. Rev. 145, 204–225.
So, R.T., Blair, N.E., Masterson, A.L., 2020. Carbonate mineral identification and quantification in sediment matrices using diffuse reflectance infrared Fourier transform spectroscopy. Environ. Chem. Lett. 18, 1725–1730.
Stanley, D.J., Hamza, F.H., 1992. Terrigenous-carbonate sediment interface (late quaternary) along the northwestern margin of the nile delta, Egypt. J. Coast Res. 153–171.
Stanley, J.-D., Goddio, F., Jorstad, T.F., Schnepp, G., 2004. Submergence of ancient Greek cities off Egypt's Nile Delta-A cautionary tale. GSA Today (Geol. Soc. Am.) 14, 4–10.
Stefaniuk, L., Morhange, C., Blanc, P.-F., Francou, S., Goiran, J.-P., 2005. Évolution des paysages littoraux dans la dépression sud-ouest de Cumes depuis 4000 ans. La question du port antique. Méditerranée. Revue géographique des pays méditerranéens/Journal of Mediterranean geography 49–59.
Stiros, S.C., Blackman, D.J., 2014. Seismic coastal uplift and subsidence in Rhodes Island, Aegean Arc: evidence from an uplifted ancient harbour. Tectonophysics 611, 114–120.
Stock, F., Pint, A., Horejs, B., Ladstätter, S., Brückner, H., 2013. In search of the harbours: new evidence of late roman and byzantine harbours of ephesus. Quat. Int. 312, 57–69.
Tsoar, H., 2000. Geomorphology and paleogeography of sand dunes that have formed the kurkar ridges in the coastal plain of Israel. Isr. J. Earth Sci. 49, 189–196.
US Army Corps of Engineers, C.E.R.C, 1984. Shore Protection Manual.
Westley, K., 2021. Satellite-derived bathymetry for maritime archaeology: testing its effectiveness at two ancient harbours in the Eastern Mediterranean. J. Archaeol. Sci.: Report 38, 103030.
Zviely, D., Kit, E., Klein, M., 2007. Longshore sand transport estimates along the Mediterranean coast of Israel in the Holocene. Mar. Geol. 238, 61–73.

Growth of the sandy isthmus of Tyre, Lebanon and ensuing relocation of its harbors

Supplementary information

S1. Leveling data on coring sites, submerged and on shore manmade structures.

The elevations of coring sites TYR1, 4, 5, 6 and of offshore markers (Fig.3) were obtained using a total station theodolite (TST) Leica TCR407ultra. Leveling was referenced to point S40 located on the modern seawall which protects the archeological site of Tyre-City (35.19469°E, 33.26788°N, WGS 84). The TST targeted an expandable 5 m-long mounting pole equipped with a prism. The offshore leveling was used to obtained the elevation of the reference point with respect to sea level on October 16th 2022 between 9 and 10 am (on a day with a tide range of 30 cm, the measurements being made during the mid-rising course). The reference point stands at an elevation of 2.95 ± 0.05 m asl. Additional repeated measurements its elevation above sea level were repeatedly conducted over the following week using a TruPulse® 360°R laser range finder. They provided an average elevation of 3.0 ± 0.15 m asl.

The elevation of coring sites TYR2 and 3 was determined in 2018 using a differential GPS Trimble Géo7x, and post-treated for atmospheric corrections. Coring site TYR7 is surrounded by tall topographic obstructions which prevented precise DGPS positioning. Its elevation was therefore obtained from the cadastral database of Tyre. The elevation of earlier coring sites [1] was reassessed using a bifrequency Leica 900 DGPS in 2019.

Site	Elevation	Longitude	Latitude	Site	Elevation	Longitude	Latitude
	cm (±2 σ)	*°E*	*°N*		*cm (±2 σ)*	*°E*	*°N*
TYR1	295 ± 6.5°	35.19480	33.26795	P1	-202 ± 7°	35.19413	33.26647
TYR2	356 ± 1 *	35.19551	33.26806	I1	-131 ± 7°	35.19601	33.26740
TYR3	623 ± 6 *	35.19459	33.27032	S1	-222 ± 7°	35.19582	33.26701
TYR4	764 ± 7°	35.19617	33.26989	S2	-135 ± 7°	35.19540	33.26747
TYR5	746 ± 7°	35.19631	33.27050	S3	-190 ± 7°	35.19616	33.26717
TYR6	676 ± 7°	35.19750	33.27158	S4	-162 ± 7°	35.19565	33.26720
TYR7	220†	35.19503	33.27292	TI	174 ± 2+	33.27353	35.19523
Q1	-227 ± 7°	35.19389	33.26642	TII	218 ± 9+	33.27315	35.24512
Q2	-215 ± 7°	35.19380	33.26645	TVIII	959 ± 10+	35.19857	35.19857
Q3	-250 ± 7°	35.19365	33.26632	TXIII	278 ± 10+	35.20162	35.20162
G1	-1.07 ± 5°	35.19424	33,26776	TXIV	944 ± 10+	35.20118	35.20118
G2	-1.84 ± 5°	35.19403	33,26728	TXV	828 ± 10+	35.20103	35.20103
M1	-196 ± 7°	35.19406	33.26692	RB	600 ± 10**	33.268-9	33.268-9
M2	-191 ± 7°	35.19476	33.26702	OC	350 ± 50**	33.269-71	33.269-71

Table S1-1. Elevation of coring sites and immersed markers. †: cadastral database of Tyre; + DGPS, 2019, °: leveling 2022; * and **: post-processed DGPS, Trimble Go7x., 2018, with *: single measurement, and **: average of the spread of elevations at street level produced by ground deformation. OC: octogonal church. RB: Roman Baths.

S2. Sand volume and sand flux calculations

Sand flux calculation:

The influence of tidal currents is negligible along the coastline of Tyre, because the tidal ranges fluctuate between 30 cm (neap tides) and 50 cm (spring tides). Longshore sediment transport, rocky shoreline erosion, sandy shoreline evolution and wind sediment transport are therefore determined by winds and waves [2]. The sandy isthmus of Tyre started to form during the Roman Climatic Optimum (200 BCE-100 CE), which climate is regarded as similar to the present-day climate (Murray, 1987). We therefore use data on the present-day wind and wave climate at Tyre (fr.wisuki.com) to assess sand fluxes at Tyre. The strongest winds (> 50 km/h) come from the southwest, with weaker winds (0-20 km/h) tracking from NW. Waves come from a narrow western sector, with some NW storms.

Littoral drift is quantified by several more or less complex formulae. The most popular and simple one was proposed by CERC (American Coastal Engineering Research Center) in 1984:

$Q = K. H^{2.5}. \sin(2\theta)$

where Q is the littoral drift (in $m^3 \cdot year^{-1}$), K a coefficient determined by wave steepness and sand grain size, H the wave height at breaking (in m), and θ the angle (in °) of incidence of waves on the coastline at the breaker line. Littoral drift is nil for wave crests parallel to the coastline (θ = 0°), increases to a wave incidence up to 45° and diminishes at higher values. At Haifa, modern longshore drift moves 50,000-80,000 $m^3 \cdot y^{-1}$ of sand northwards [3], for a mean incidence angle of waves of θ = 10°. Assuming that sand transport at Haifa and occurs at transport capacity, the decrease in the incidence angle to θ = 6° at Tyre implies that longshore transport capacity at Tyre is 30-50,000 $m^3 \cdot y^{-1}$. We further assume that sand influx is not limited by the sand production capacity of the source area, and therefore than sand influx at Tyre occurs at transport capacity.

Sand volume calculation.

The total volume of sand accumulated behind Tyre Island was calculated as the difference (Fig. S2-4) between the elevation of the modern onshore and offshore surface of the sandy isthmus (Fig. S2-3) and the elevation of the substrate over which the sands were deposited (Fig. S2-1). The substrate comprises lagoonal clays laid down between the ridge of Tyre and the mainland during the marine transgression [4], of the calcarenite forming the ridge of Tyre, and of seaward-dipping calcarenite beds along the mainland coast. This composite basement was intersected by coring along the isthmus of Tyre. Offshore, it crops out on the sea floor, north and south of the area of accumulation of the bioclastic sands forming the sandy isthmus (dashed line, Fig. S2-1,2, and 3).

The volume of sand accumulated behind Tyre Island by 330 BCE (Fig. S2-4) was calculated as the difference between a reconstruction of the sand bank as in 330 BCE (Fig. S2-2), and the elevation of the previously described substrate (Fig. S2-1). To reconstruct the sand bank in 332 BCE, we assumed that the elevation of its ridgeline is constrained by the depth of the 300 BCE isochron in the sand unit, as found in cores along the sandy isthmus (Fig. 6B). Its northern and southern flanks slopes were reconstructed the modern northern and southern beach profiles of the peninsula, as provided by the multibeam data (Fig.2, MarEA/EAMENA database, data GEOARCH-0000114).

The volume of sand accumulated since the construction of Alexander's causeway is the difference between the total volume of sand and the sand accumulated before 330 BC (Fig.S2-6). This

volume of 30.10^6 m^3, comprises of 10.10^6 m^3 deposited in the sea and 20.10^6 m^3 deposited subaerially (assuming no change in sea level), requires 6-10 centuries to be built at a rate of 30,000 to 50,000 $m^3.y^{-1}$.

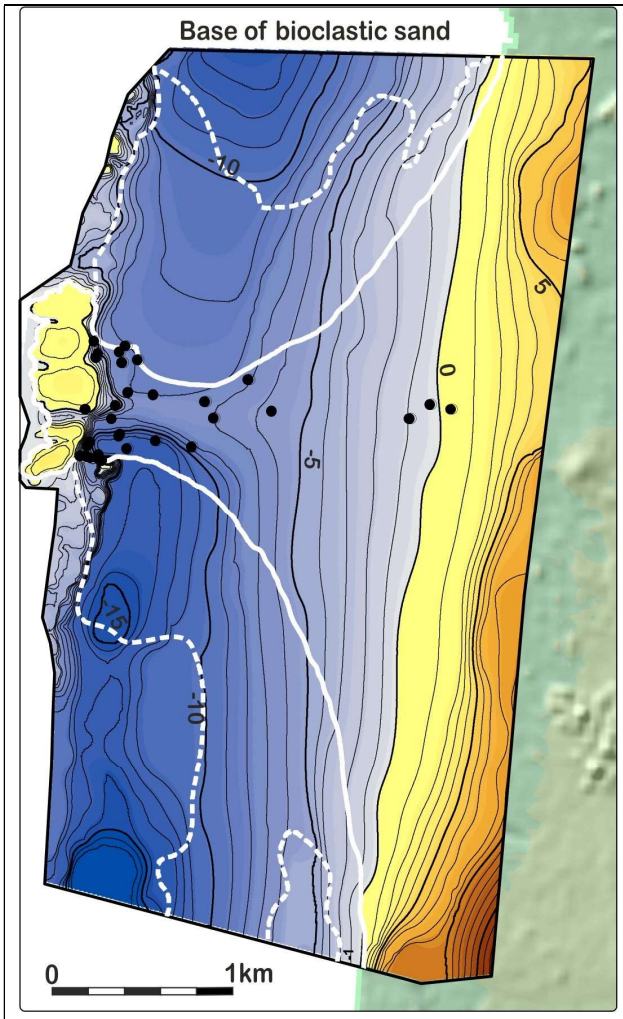

Figure S2-1. Base of the sands below the isthmus

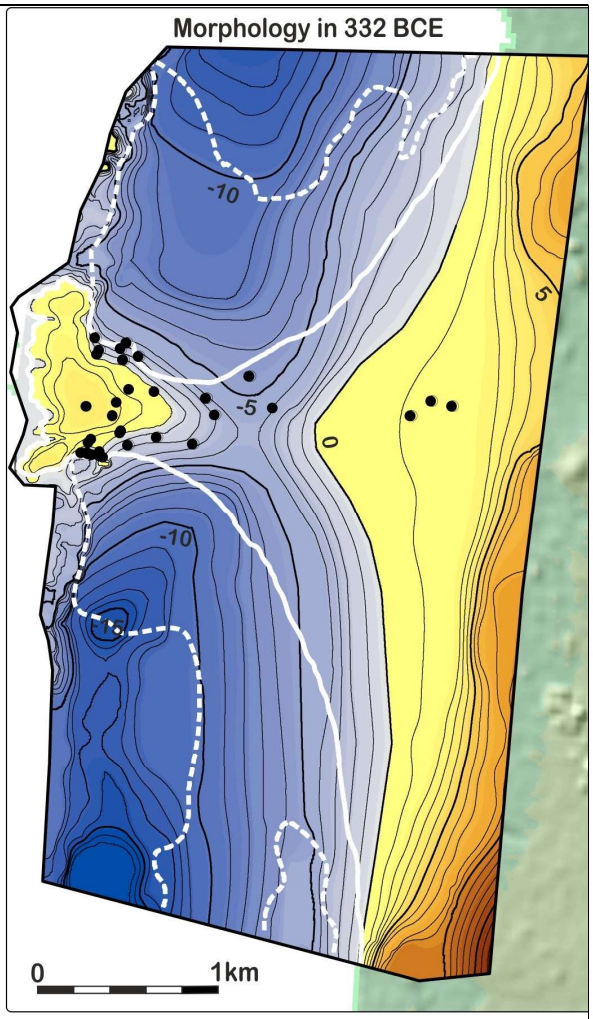

Figure S2-2. Topography of the sand bank in 332 BCE

Black dots: core locations. Solid white line: present-day coastline. Dashed white line: present-day outer boundaries of the sand accumulation associated to the isthmus.

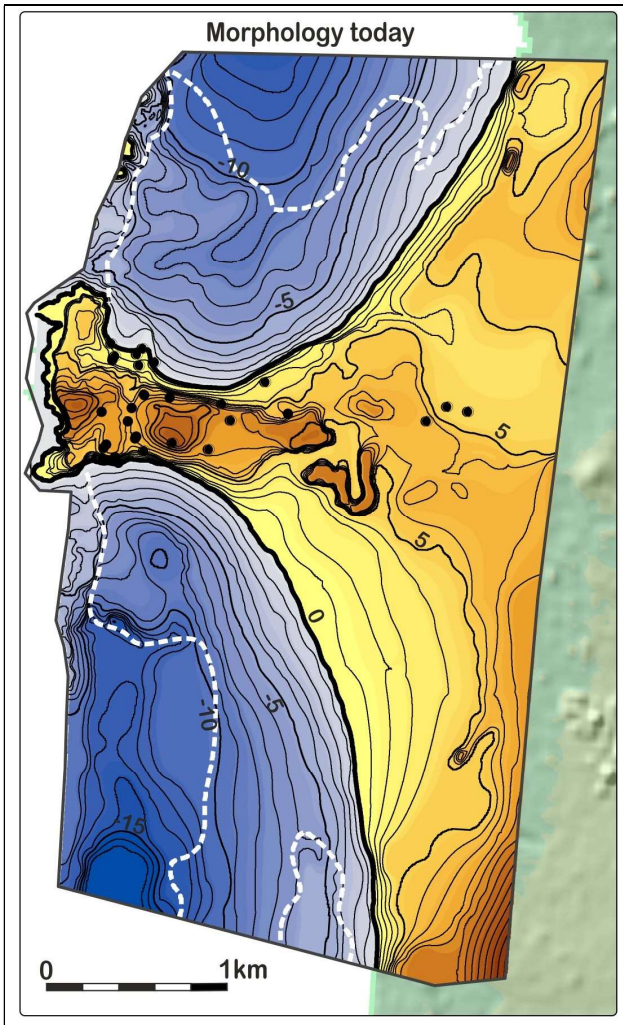

Figure S2-3. Modern topography of the isthmus

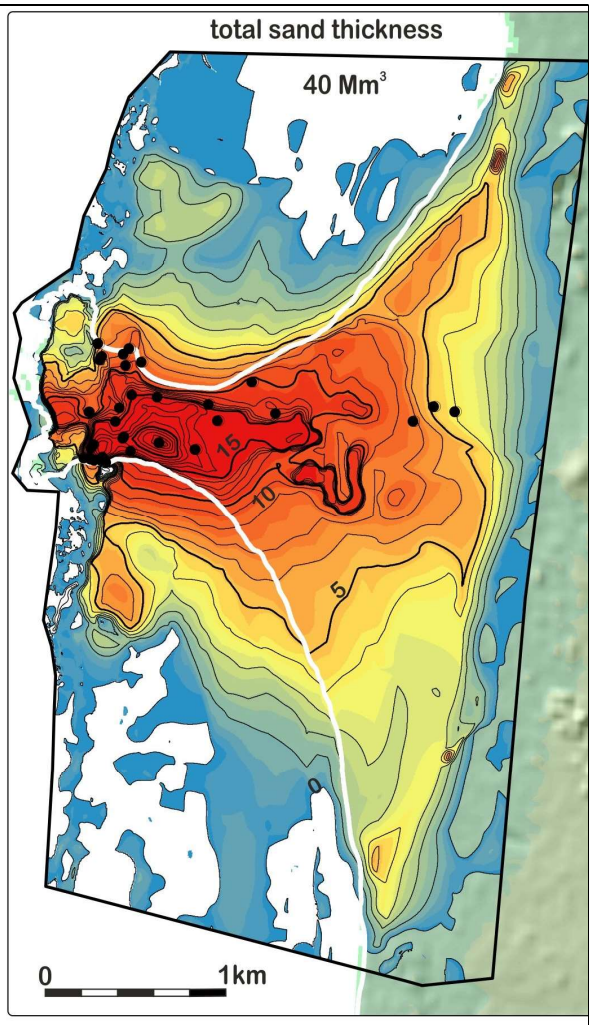

Figure S2-4. Total sand thickness

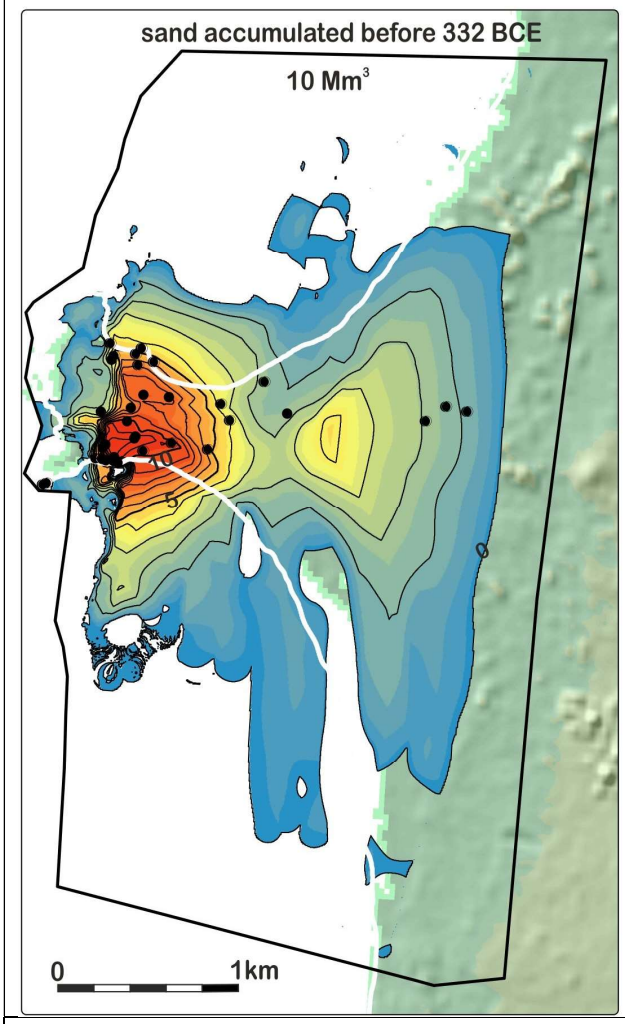

Figure S2-5. Thickness of sand deposited before 330 BCE

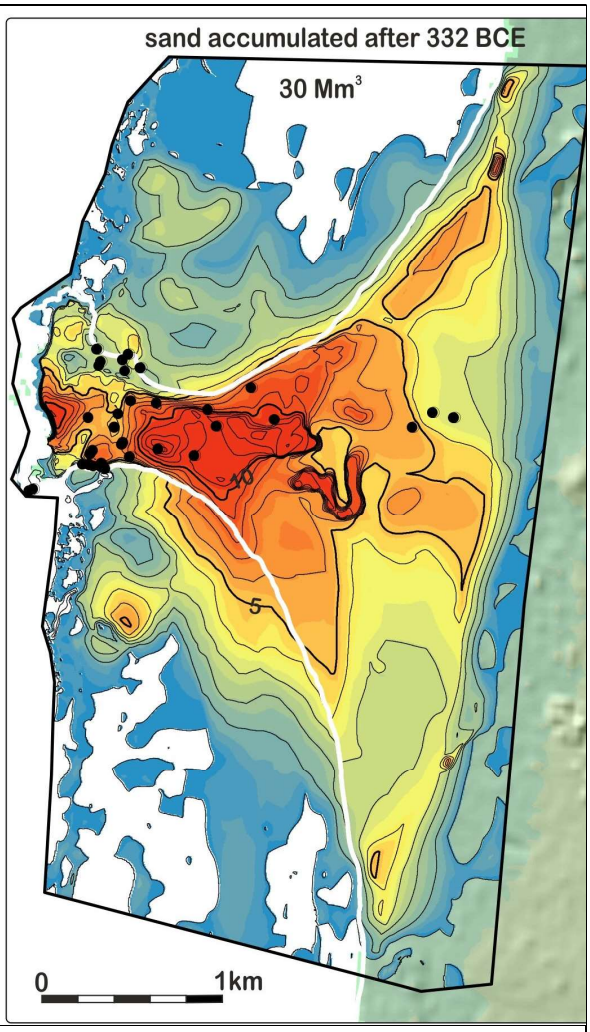

Figure S2-6. Thickness of sand deposited after 330 BCE

S3. Radiocarbon dating and calibration

Core	Name	Nature	Lab. #	Elevation asl	Age BP	Calendar age
				(m)	year BP	year CE (min max)
TYR4	7.4-7.7	charred wood	Ly17468	0.1 ± 0.2	2,220 ± 30	-385 -197
TYR4	11.4-11.6	plant	Ly17467	-3.9 ± 0.2	2,935 ± 30	-1256 -1017
TYR4	16.5-16.6	charred wood	Ly17450	-8.9 ± 0.1	6,045 ± 40	-5198 -4805
TYR4	17.1-17.2	charred wood	Ly17466	-9.5 ± 0.1	5,860 ± 35	-4833 -4612
TYR4	17.5-17.6	wood	Ly17451	-9.9 ± 0.1	5,820 ± 35	-4785 -4551
TYR5	8.25-8.5	Shell*	Ly16034	-0.9 ± 0.2	2,600 ± 30	-341 -6
TYR5	8.5-9.0	bone	Ly18789	-1.3 ± 0.3	2,280 ± 30	-401 -208
TYR5	9.8-10.0	seed	Ly18790	-2.4 ± 0.2	2,320 ± 30	-459 -231
TYR5	12.5-12.6	seed	Ly17463	-5.1 ± 0.1	2,740 ± 30	-956 -813
TYR5	12.8-12.9	charred wood	Ly17465	-5.4 ± 0.1	2,520 ± 30	-725 -544
TYR6	7.2-7.3	charred wood	Ly18738	0.5 ± 0.1	1,790 ± 30	-353 -206
TYR6	7.8-8.0	charred wood	Ly18739	-1.1 ± 0.2	2,240 ± 30	-390 -202
TYR6	9.0-9.1	micro-char	Ly18791	-2.3 ± 0.1	2,240 ± 30	-390 -202
TYR6	9.3-9.5	charred wood	Ly18740	-2.6 ± 0.2	2,200 ± 30	-368 -173
TYR6	11.5	bone	Ly18792	-4.7 ± 0.1	2,890 ± 30	-1203 -941
TYR7	3.6-3.7	charred wood	Ly18793	-1.5 ± 0.3	1,290 ± 30	660 776
TYR7	4.7-4.8	seed	Ly18794	-2.6 ± 0.3	2,060 ± 30	-162 17

Table S3-1. Radiocarbon ages of cores TYR4-7. Ages (2σ) calculated using the online software Oxcal v. 4.4 (https://c14.arch.ox.ac.uk/oxcal.html) using the continental calibration curve of Reimer Reimer, Austin [5], except (*): marine calibration curve of Heaton, Köhler [6].

Core	Name	Nature	Lab. #	Elevation asl	Age BP	Calendar age
				(m)	year BP	year CE (min max,)
T1	4	Cyclope neritea*	Lyon-1469	-0.3	1,560 ± 35	850 1,160
T1	12	Cyclope neritea*	Lyon-1470	-1.3	1,965 ± 35	438 712
T1	24	Loripes lacteus*	Lyon-1472	-2.1	2,255 ±35	113 426
T1	30	Cyclope neritea*	Lyon-1471	-3.0	2,055 ± 35	353 645
T1	31	Nassarius pygmaeus*	Lyon-1602	-3.1	2,635 ± 45	-376 -31
T1	36	Mitra cornicula*	Lyon-1603	-4.6	5,520 ± 50	-3,943 -3,600
T1	39	Cyclope neritea*	Lyon-1473	-0.3	2,375 ± 30	-44 276
T5	19	charcoal	Poz-2500	-2.9	1,485 ± 30	530 650
T5	41	charcoal	Poz-2502	-3.5	1,910 ± 30	20 180
T5	43	charcoal	Poz-5768	-4.9	2,265 ± 30	-400 -200
T5	58	Nassarius mutabilis*	Poz-5752	-5.1	2,360 ± 30	-110 60
T5	60	charcoal	Poz-5769	-6.0	2,245 ± 35	-400 -200
T5	70	Cerithium vulgatum*	Poz-2445	-6.3	5,730 ± 30	-4,290 -4,080
T5	76	Cerithium vulgatum*	Poz-2451	-6.4	6,400 ± 35	-5,020 -4,800
T5	77	Cerithium vulgatum*	Poz-2446	-6.5	7,300 ± 40	-5,890 -5,710
T5	81	Cerithium vulgatum*	Poz-2447	-6.5	7,760 ± 40	-6,380 -6,180
T5	82	Cerithium vulgatum*	Poz-2448	-7.3	7,780 ± 40	-6,390 -6,200
T5	106	Cerithium vulgatum*	Poz-2449	-2.9	7,800 ± 40	-6,400 -6,210
T6	na	marine*	na	-4.8	225 ± 30	1,866 1,950
T6	na	marine*	na	-8.6	2,120 ± 30	266 570
T6	na	marine*	na	-10.8	6,065 ± 30	-4,501 -4,202
T8	na	marine*	na	0	2,510 ± 30	-200 123
T8	na	marine*	na	-7.5	6,300 ± 40	-4,773 -4,427
T9	6	olive seed	Poz-5770	-3.8	1,615 ± 30	410 542
T9	20	grape seeds	Poz-5773	-4.8	1,855 ± 30	89 245

T9	25	Nassarius mutabilis*	Poz-5774	-5.4	2,220 ± 35	150 451
T9	26	seed	Poz-5777	-5.6	2,385 ± 30	-719 -393
T9	35Ch	charcoal	Poz-5775	-6.5	2,215 ± 30	-381 -197
T9	35Co	Loripes lacteus*	Poz-5778	-6.5	2,505 ± 30	-196 126
T9	43	seed	Poz-5779	-7.2	2,055 ± 30	-160 22
T9	45	charcoal	Poz-5780	-7.5	2,320 ± 35	-481 -210
T9	49	Cyclope neritea*	Poz-5781	-7.7	2,140 ± 30	254 552
T9	52	Donax*	Poz-7184	-8.2	2,210 ± 30	165 469
T9	53	Donax venustus*	Poz-5783	-8.4	2,300 ± 30	60 374
T9	62	Loripes lacteus*	Poz-5784	-9.1	5,850 ± 40	-4,301 -3,953
T9	63	Loripes lacteus*	Poz-5784	-9.3	5,830 ± 40	-4,266 -3,936
T9	76	Parvicardium exiguum*	Poz-5785	-10.8	7,840 ± 40	-6,352 -6,014
T13	9	Tricolia pullus*	Poz-9943	-2.5	2,650 ± 35	-376 -57
T13	15	Rissoa*	Poz-9898	-3.6	2,870 ± 30	-701 -358
T13	21	Rissoa*	Poz-9944	-5.2	2,980 ± 35	-787 -461
T13	25	Loripes lacteus*	Poz-9945	-6.5	7,450 ± 40	-5,927 -5,626
T13	39	Parvicardium exiguum*	Poz-13916	-2.5	7,210 ± 40	-5,696 -5,411
T14	6	Donax semistriatus*	Poz-13964	-1.6	2,245 ± 30	130 427
T14	14	Tricolia pullus*	Poz-12137	-4.1	2,795 ± 30	-581 -220
T14	20	Venus casina*	Poz-13915	-6.8	6,370 ± 35	-4,840 -4,496
T14	23	Loripes lacteus*	Poz-12136	-9.4	7,840 ± 40	-6,342 -6,022
T15	19	Nassarius reticulatus*	Poz-12154	-1.5	2,385 ± 30	-43 260
T15	25	Mitra ebenus*	Poz-13965	-5.1	5,775 ± 35	-4,226 -3,886
T15	26	Cerithium vulgatum*	Poz-12133	-5.9	5,740 ± 35	-4,178 -3,815
T15	30	Parvicardium exiguum*	Poz-12134	-8.5	7,680 ± 40	-6,179 -5,855
T18	39	Parvicardium exiguum*	Poz-13966	-2.2	4,180 ± 30	-2,293 -1,940
T18	59	Neverita josphinae*	Poz-9946	-3.8	5,710 ± 40	-4,154 -3,785
T18	64	L. Lacteus*	Poz-9900	-4.8	5,980 ± 40	-4,416 -4,072

Table S3-2. Radiocarbon ages of cores T1, T5, T6,T8, T9,T13,T14,T15, and T18 [1, 4, 7] used in the present synthesis. Ages (2σ) calculated using the online software Oxcal v. 4.4 (https://c14.arch.ox.ac.uk/oxcal.html) using the continental calibration curve of Reimer, Austin [5] et al., 2020, except for (*): marine calibration curve of Heaton, Köhler [6]et al., 2020, with a reservoir age (R) of 550 years.

S4. Sand carbonate content and strontium isotopic ratios

We used mid-infrared absorbance spectroscopy to determine carbonate abundance in 24 sand and sandy clay samples from cores TYR1 (n=2), TYR2 (n=4), TYR4 (n=5), TYR5 (n=9), and TYR6 (n=4). The samples were oven-dried at 50°C for seven days. 10 g of each sample were then wet-sieved through stainless steel meshes to extract the sand fraction (63µm- 2 mm). Wet sieving eliminates silt and clay coatings from the sand grains. The sandy fraction was then ground using an agate mortar and pestle. The fine powder was then oven-dried at 50°C for 24h prior to measurement.

20 mg of each powdered sample were then placed into a FT-IR Frontier Spectrometer, equipped with a KBr beam splitter, a diffuse reflectance sampling accessory, and a triglycine sulphate detector (PerkinElmer, Waltham, MA, USA). Absorbance was measured from 4,000 to 450 cm^{-1}, by 2 cm^{-1} increments. Measurements were made against a background sample composed of dried powdered potassium bromide (KBr). Measurements were conducted at the analytical platform of Archéorient – UMR 5133 at Jalès, Ardèche, France.

Core	Sample	Elevation	Carbonate	Core	Sample	Elevation	Carbonate
		(m) 2 σ	*% wt 2 σ*			*(m) 2 σ*	% wt
TYR1	2.0-3.0	0.5 ± 0.6	98 ± 3	TYR5	9.8-10.0	-1.3 ± 0.3	96 ± 3
TYR1	3.5-4.5	-0.5 ± 0.6	92 ± 3	TYR5	11.85-11.9	-4.4 ± 0.3	95 ± 3
TYR2	5.25-5.43	-2.2 ± 0.3	65 ± 3	TYR5	11.9-11.95	-4.5 ± 0.2	86 ± 3
TYR2	5.8-6.0	-2.8 ± 0.2	87 ± 3	TYR5	12.0-12.5	-4.6 ± 0.3	92 ± 3
TYR2	7.0-7.3	-4.0 ± 0.3	94 ± 3	TYR5	13.1-13.2	-5.7 ± 0.2	100 ± 3
TYR2	7.75-8.0	-4.7 ± 0.3	90 ± 3	TYR5	14.9-15.0	-7.5 ± 0.2	58 ± 3
TYR4	7.7-7.8	- 0.1 ±0.2	100 ± 3	TYR5	16.75-17.0	-9.4 ± 0.4	75 ± 3
TYR4	9.0-9.4	-1.6 ± 0.5	94 ± 3	TYR5	19.0*	-11.5 ± 0.1	53 ± 3
TYR4	10.0-10.3	-2.5 ± 0.4	90 ± 3	TYR6	7.0-7.1	-0.3 ± 0.4	88 ± 3
TYR4	10.8-11.0	-3.3 ± 0.3	100 ± 3	TYR6	7.7-7.8	-1.0 ± 0.3	92 ± 3
TYR4	17.9-18.0*	-10.3 ± 0.2	11 ± 3	TYR6	9.2-9.3	-2.5 ± 0.3	81 ± 3
TYR5	8.25	- 0.8 ± 0.2	76 ± 3	TYR6	11.2-11.3	-4.5 ± 0.2	100 ± 3

Table S4-1. Carbonate content of the sands from the isthmus of Tyre, determined by MIRS. *: sandy fraction of the clay layer below the sandy isthmus.

^{87}Sr (strontium) is produced by the disintegration of a parent ^{87}Rb (rubidium) isotope with a half-life of 48.8 Gy. The relative abundances of strontium isotopes evolve over geologic time by progressive addition of radiogenic ^{37}Sr. Strontium is easily incorporated into calcite and aragonite, unlike rubidium. The $^{87}Sr/^{86}Sr$ composition of marine carbonates reflects the composition of seawater at their time of crystallization, because no ^{87}Rb is incorporated in the carbonates. The $^{37}Sr/^{36}Sr$ of sea water has increased since Jurassic times, from 0.707327366 during the Jurassic, to 0.707580388 during the Cretaceous, 0.707732946 during the Eocene, 0.709167 during in Middle Pleistocene, and 0.709174 today. Owing to this, $^{87}Sr/^{86}Sr$ has been used to conduct stratigraphic correlations and marine carbonate dating [8]. It has also been used as a tracer of rock source type/age [9].

The sand fraction (63 µm-2 mm) was extracted by wet sieving at the Jalès laboratory of Archéorient, University of Lyon. Between 20 and 70 mg of each sample were dissolved using 0.5 ml of 3N HNO_3. The dissolved $CaCO_3$ fraction was extracted by centrifugation. Strontium was separated on ion exchange columns using a Sr Spec resin (Eichrom Technologies Inc.) by nitric leaching, using a

protocol modified from Pin and Bassin [10]. The purified sample was diluted in 0.5N nitric acid to reach a Sr concentration of 20 ppb. The isotopic composition of the samples was then measured at the Laboratoire des Sciences du Climat et de l'Environnement (LSCE, France) on a ThermoScientific ™ Neptune Plus ™ Multi-Collector Inductively Coupled Plasma Mass Spectrometer (MC-ICPMS), fitted with a desolvating system APEX Omega. After correction for blanks and isotopic interferences (with Kr and Rb), isotopic $^{87}Sr/^{86}Sr$ ratios were corrected for mass fractionation assuming a constant $^{88}Sr/^{86}Sr$= 8.375209. Isotopic ratios were further corrected using a sample-bracketing method with NBS 987 value (0.710245 ± 0.00003). Over the course of the analysis, measurements of reference standards JCt-1 and Durango yielded $^{87}Sr/^{86}Sr$ ratio values of 0.709165 (n=3, stdev at 2 s = 14 ppm), and 0.706357 (n = 3 stdev at 2 s = 29 ppm), respectively.

Core	Sample	Lab #	$^{37}Sr/^{36}Sr$	(2σ 10^{-6})	Core	Sample	Lab #	$^{37}Sr/^{36}Sr$	(2σ 10^{-6})
TYR 4	1.0-2.0	8686	0.709057	(10)	TYR 5	16.00-16.25	8695	0.709134	(10)
TYR 4	4.5	8687	0.709045	(12)	TYR 6	5.0-6.0	8696	0.708170	(22)
TYR 4	7.0-7.3	8688	0.709099	(10)	TYR 6	5.0-6.0*	8696	0.708171	(31)
TYR 4	9.4-9.7	8689	0.709148	(10)	TYR 6	7.4-7.5	8698	0.708743	(27)
TYR 4	11.6-11.8	8948	0.709154	(14)	TYR 6	7.4-7.5*	8698	0.708827	(11)
TYR 4	16.9-17.0	8691	0.709142	(11)	TYR 6	11.2-11.3*	8950	0.709117	(13)
TYR 5	9.8-10.0	8693	0.709101	(10)	TYR 6	14.9-15.0	8950	0.709130	(14)
TYR 5	12.00-12.05	8694	0.709116	(11)	TYR 6	15.0-15.1	8952	0.709123	(14)

Table S4-2. Isotopic ratios of carbonate sands from the isthmus of Tyre. The 2 σ uncertainty on $^{87}Sr/^{86}Sr$ values, reported in brackets as part per million, combines the reproducibility of the session standards and the measurement error of each sample. * replication of the measurement on the finer fraction of the sediment.

References

1. Marriner N, Goiran J, Morhange C. Alexander the Great's tombolos at Tyre and Alexandria, eastern Mediterranean. Geomorphology. 2008;100(3-4):377-400.
2. Nir Y. The city of Tyre, Lebanon and its semi-artificial tombolo. Geoarchaeology. 1996;11(3):235-50.
3. Zviely D, Kit E, Klein M. Longshore sand transport estimates along the Mediterranean coast of Israel in the Holocene. Marine Geology. 2007;238(1-4):61-73.
4. Marriner N, Morhange C, Meulé S. Holocene morphogenesis of Alexander the Great's isthmus at Tyre in Lebanon. Proceedings of the National Academy of Sciences. 2007;104(22):9218-23.
5. Reimer PJ, Austin WE, Bard E, Bayliss A, Blackwell PG, Ramsey CB, et al. The IntCal20 Northern Hemisphere radiocarbon age calibration curve (0–55 cal kBP). Radiocarbon. 2020;62(4):725-57.
6. Heaton TJ, Köhler P, Butzin M, Bard E, Reimer RW, Austin WE, et al. Marine20—the marine radiocarbon age calibration curve (0–55,000 cal BP). Radiocarbon. 2020;62(4):779-820.
7. Marriner N, Morhange C, Boudagher-Fadel M, Bourcier M, Carbonel P. Geoarchaeology of Tyre's ancient northern harbour, Phoenicia. Journal of Archaeological Science. 2005;32(9):1302-27.
8. Elderfield H. Strontium isotope stratigraphy. Palaeogeography, palaeoclimatology, palaeoecology. 1986;57(1):71-90.
9. Bayon G, Freslon N, Germain Y, Bindeman IN, Trinquier A, Barrat J-A. A global survey of radiogenic strontium isotopes in river sediments. Chemical Geology. 2021;559:119958.
10. Pin C, Bassin C. Evaluation of a strontium-specific extraction chromatographic method for isotopic analysis in geological materials. Analytica Chimica Acta. 1992;269(2):249-55.